Am J Cancer Res 2023;13(12):6313-6332
www.ajcr.us /ISSN:2156-6976/ajcr0153534

*Original Article*

# The critical roles of lnc-GLYATL2-2/PD-L1 axis in immune microenvironment and the clinical value of intracranial chordomas

Chengbin Wang[1], Yingliang Liu[1], Daming Cui[1], Yang Jiang[1], Li Li[2]

*[1]Department of Neurosurgery, Shanghai Tenth People's Hospital, Tongji University School of Medicine, Shanghai 200072, China; [2]Hospital for Chronic Neurological Diseases, Xi'an International Meidical Center Hospital Affiliated to Northwest University, Xi'an 710000, Shaanxi, China*

Received September 20, 2023; Accepted December 15, 2023; Epub December 15, 2023; Published December 30, 2023

**Abstract:** Intracranial chordomas (ICs) are associated with a poor prognosis due to low total resection rates and high recurrence rates. However, the role of immunotherapy in ICs remains unknown. RNA sequencing and immunohistochemical staining were performed on IC tissues and normal tissues, and the long noncoding RNA (lncRNA) lnc-GLYATL2-2 was identified. The results indicated that high expression of lnc-GLYATL2-2 was positively correlated with the tumor-infiltrating lymphocyte (TIL) markers CD4 and Foxp3, negatively correlated with CD8, and positively correlated with the expression of the immune checkpoint molecules programmed death receptor-1 (PD-1) and programmed death ligand 1 (PD-L1). Additionally, Kaplan-Meier and univariate or multivariate Cox regression analyses revealed the predictive value of lnc-GLYATL2-2 for survival based on clinical data from patients with ICs. A high expression level of lnc-GLYATL2-2 is potentially correlated with a suppressive tumor immune microenvironment and adverse clinical outcomes in IC patients. Mechanistically, the upregulation of lnc-GLYATL2-2 can result in increased cytoplasmic levels of ELAVL1, leading to enhanced binding to the 3'-UTR of PD-L1 mRNA and maintenance of its stability. In contrast, lnc-GLYATL2-2 can directly interact with the PD-L1 protein to prevent degradation, thereby promoting high levels of PD-L1 expression simultaneously at the transcriptional and translational levels in chordoma cells. These results provide a new perspective on the diagnosis and prognosis of ICs and provide theoretical evidence for immunotherapy in patients with ICs.

**Keywords:** Intracranial chordomas, PD-L1, Lnc-GLYATL2-2, ELAVL1

## Introduction

Chordomas are rare tumors originating from embryonic remnants of the notochord and can occur at any site, most commonly in the sacrococcygeal region (45%) or clivus at the skull base (40%) [1]. Intracranial chordomas (ICs) have an insidious onset and are challenging to diagnose at an early stage [2, 3]. ICs often invade a wide range of bones in the midline of the skull base and involve multiple pairs of cranial nerves and large vessels, resulting in an unsatisfactory surgical exposure and low total resection rates [1, 4]. Because of their weak response to conventional radiotherapy and chemotherapy, most IC patients have a poor prognosis, with a 5-year survival rate of 65% [5, 6]. Currently, the clinical treatment for ICs is maximal surgical resection supplemented by radiotherapy. There has been active progress in targeted therapy and immunotherapy [7, 8]. Therefore, it is essential to explore the molecular regulatory mechanisms of chordoma and discover potential therapeutic targets that can improve the prognosis of patients with ICs.

Solid tumors can employ various strategies to adapt to the immune microenvironment and resist the body's immune attack [9]. The PD1-PDL1 pathway mediates tumor immune escape by inducing apoptosis in tumor-infiltrating lymphocytes and immunosuppression in a variety of solid tumors, such as breast cancer, non-small cell lung cancer, and melanoma [10]. Blocking the binding of PD-L1 to its receptor PD1 with antibodies (anti-PD therapy) can lead

to remission in a proportion of patients with advanced cancer [11]. However, the application of anti-PD therapy for the treatment of ICs has rarely been reported, and the effectiveness of immunotherapy for treating ICs has not been determined.

Long noncoding RNAs (LncRNAs) are heterogeneous RNAs that are more than 200 nucleotides in length and do not have the potential for protein coding [12]. LncRNAs have been confirmed to exert diverse cellular functions, including cis- or trans-transcriptional regulation as well as post-transcriptional modulation, by interacting with miRNAs, mRNAs, or proteins [13]. Emerging evidence suggests that lncRNAs are associated with multiple features of tumors, such as proliferation, invasion, metastasis, and treatment resistance [14-16]. Recent studies have indicated that several lncRNAs that promote or inhibit cancer progression not only play a role in malignant cells but also affect the function of tumor-specific immune cells, thereby reshaping the tumor immune microenvironment (TIME) [17, 18]. LncRNAs are involved in and regulate critical mechanisms of tumor immunity, ranging from antigen presentation to T-cell depletion [19, 20]. These molecules have been characterized for their diagnostic and prognostic value, but how to remodel the TIME in ICs has not been fully elucidated.

RNA-binding proteins (RBPs) are a crucial class of proteins in cells that play important roles in RNA stability, pre-mRNA splicing, and translational processes by specifically recognizing RNA. Dysregulation of RBPs can lead to the occurrence of various diseases, including human cancers [21]. ELAVL1, a critical protein, typically binds to mRNAs containing adenylate-uridylate-rich elements (AREs) found in the 3' untranslated region (3'UTR). The binding of the ELAVL1 protein to the ARE can significantly increase the half-life and stability of the corresponding mRNAs [22].

In this study, we analyzed RNA-seq data from ICs to mine and identify functional lncRNAs associated with the tumor microenvironment. We identified a novel lncRNA, lnc-GLYATL2-2, which is closely related to PD-L1 expression levels, microenvironmental tumor-infiltrating lymphocytes (TILs), and clinicopathological features in chordoma cells. In addition, a high lnc-GLYATL2-2/CD8 ratio and high infiltration of PD-1$^+$ TILs suggested shorter local recurrence-free survival (LRFS) and overall survival (OS) in patients with ICs. Mechanistically, lnc-GLYATL2-2 can simultaneously regulate the expression of PD-L1 at the transcriptional and translational levels, thus maintaining high levels of PD-L1 expression in chordoma. Additionally, lnc-GLYATL2-2 may serve as a predictor of immunotherapy responsiveness in patients with ICs.

## Methods

### *Patients and tumor specimens*

Tumor specimens were collected retrospectively from 96 patients with intracranial chordomas who underwent surgery in our department between June 2014 and April 2022. As normal controls, 7 nucleus pulposus tissue samples were also retrieved from aborted fetuses gestationally aged 8-24 weeks in the Department of Gynecology and Obstetrics [23]. Patients who had previously received chemotherapy, radiotherapy or any other type of tumor-specific therapy were excluded from this study. Clinicopathologic data, including age, sex, tumor size, location [24], tumor invasion, preoperative recurrence, and type of resection, are shown in **Table 1**. This study was performed with the permission of the Ethics Committee of our hospital.

Due to the peculiarity of the growth site of intracranial chordomas, gross resection is almost impossible. In this study, progression of chordoma was defined as recurrence or regrowth of the residual tumor. The pathological diagnosis of chordoma was confirmed by two practicing pathologists by reviewing the histopathological examination of hematoxylin and eosin (HE)-stained tumor tissue sections [25]. Therefore, the pathological types of intracranial chordoma in this study included only conventional and chondroid types. To describe the resection range of chordomas, we defined the extent of tumor resection as follows: > 90% total resection and subtotal resection and ≤ 90% partial resection and biopsy. Tumor invasion was defined as chordoma infiltrating adjacent skeletal or dural structures and was assessed mainly by MRI and CT imaging [26]. All included patients underwent preoperative MRI or CT to determine the presence of tumor invasion.

**Table 1.** The relationships between Lnc-GLYATL2-2, PD-L1, TILs and clinicopathological features of ICs patients

| Clinicopathological features | PD-1$^+$ TILs | | | PD-L1 expression | | | Lnc-GLYATL2-2 expression | | | CD8$^+$ TILs | | | CD4$^+$ TILs | | | Foxp3$^+$ TILs | | |
|---|---|---|---|---|---|---|---|---|---|---|---|---|---|---|---|---|---|---|
| | No. of patients (n=96) | Mean ± SD | *p* values | Negative (n=19) | Positive (n=77) | *p* values | No. of patients (n=96) | Mean ± SD | *p* values | No. of patients (n=96) | Mean ± SD | *p* values | No. of patients (n=96) | Mean ± SD | *p* values | No. of patients (n=96) | Mean ± SD | *p* values |
| Age (years) | | | | | | | | | | | | | | | | | | |
| ≤ 50 | 49 | 233.6±52.2 | 0.372 | 7 | 42 | 0.167 | 49 | 4.33±2.18 | 0.761 | 49 | 388.6±42.9 | 0.094 | 49 | 238.1±39.2 | 0.417 | 49 | 162.4±30.5 | 0.539 |
| > 50 | 47 | 243.3±53.8 | | 12 | 35 | | 47 | 4.19±2.32 | | 47 | 373.4±45.1 | | 47 | 244.2±33.7 | | 47 | 166.2±29.8 | |
| Sex | | | | | | | | | | | | | | | | | | |
| Male | 56 | 239.4±51.5 | 0.358 | 11 | 45 | 0.965 | 56 | 4.01±2.53 | 0.593 | 56 | 385.2±45.6 | 0.546 | 56 | 245.3±32.5 | 0.526 | 56 | 174.1±25.8 | 0.091 |
| Female | 40 | 249.1±49.6 | | 8 | 32 | | 40 | 4.27±2.05 | | 40 | 391.1±49.1 | | 40 | 249.8±36.4 | | 40 | 165.3±23.5 | |
| Tumor size (cm) | | | | | | | | | | | | | | | | | | |
| ≤ 4 | 39 | 232.7±47.3 | 0.412 | 9 | 30 | 0.504 | 39 | 3.97±2.11 | 0.249 | 39 | 402.7±46.4 | 0.152 | 39 | 257.2±37.6 | 0.199 | 39 | 169.7±34.4 | 0.212 |
| > 4 | 57 | 241.1±50.2 | | 10 | 47 | | 57 | 4.52±2.39 | | 57 | 389.5±42.2 | | 57 | 246.9±38.8 | | 57 | 178.5±33.2 | |
| Location | | | | | | | | | | | | | | | | | | |
| Superior clivus | 41 | 244.2±55.1 | 0.871 | 11 | 30 | 0.318 | 41 | 4.47±2.24 | 0.746 | 41 | 384.1±47.9 | 0.493 | 41 | 253.2±36.7 | 0.254 | 41 | 163.5±32.5 | 0.712 |
| Middle clivus | 32 | 247.3±49.3 | | 5 | 27 | | 32 | 4.72±2.63 | | 32 | 370.7±48.7 | | 32 | 239.4±34.6 | | 32 | 169.2±38.9 | |
| Inferior clivus | 23 | 251.6±58.4 | | 3 | 20 | | 23 | 4.21±2.51 | | 23 | 379.4±46.2 | | 23 | 247.5±32.7 | | 23 | 170.2±38.5 | |
| Invasion condition | | | | | | | | | | | | | | | | | | |
| Yes | 72 | 255.4±53.3 | < 0.001 | 10 | 62 | 0.012 | 72 | 5.26±1.38 | 0.002 | 72 | 390.2±48.1 | 0.256 | 72 | 255.6±33.1 | 0.254 | 72 | 177.3±36.2 | 0.658 |
| No | 24 | 211.8±52.8 | | 9 | 15 | | 24 | 4.06±2.03 | | 24 | 377.4±45.6 | | 24 | 246.4±36.7 | | 24 | 173.6±32.8 | |
| Preoperative recurrence | | | | | | | | | | | | | | | | | | |
| Yes | 68 | 242.5±56.3 | 0.886 | 13 | 55 | 0.796 | 68 | 4.39±2.41 | 0.656 | 68 | 378.7±44.3 | 0.599 | 68 | 235.4±39.3 | 0.585 | 68 | 159.4±39.2 | 0.112 |
| No | 28 | 240.7±55.2 | | 6 | 22 | | 28 | 4.16±1.97 | | 28 | 383.9±42.7 | | 28 | 240.1±35.4 | | 28 | 172.9±32.7 | |
| Rate of resection | | | | | | | | | | | | | | | | | | |
| ≤ 90% | 54 | 238.8±49.3 | 0.905 | 9 | 45 | 0.384 | 54 | 4.63±2.46 | 0.264 | 54 | 366.5±47.3 | 0.172 | 54 | 250.9±33.7 | 0.414 | 54 | 172.6±34.5 | 0.748 |
| > 90% | 42 | 237.6±47.8 | | 10 | 32 | | 42 | 4.07±2.37 | | 42 | 379.6±44.9 | | 42 | 256.5±32.4 | | 42 | 170.4±31.3 | |
| Histopathology | | | | | | | | | | | | | | | | | | |
| Conventional | 71 | 246.5±58.2 | 0.899 | 15 | 56 | 0.58 | 71 | 4.35±2.77 | 0.513 | 71 | 393.3±42.9 | 0.427 | 71 | 251.7±34.3 | 0.369 | 71 | 168.8±36.9 | 0.610 |
| Chondroid | 25 | 248.2±55.7 | | 4 | 21 | | 25 | 3.95±2.13 | | 25 | 385.1±47.8 | | 25 | 244.2±39.6 | | 25 | 173.1±33.7 | |

*Follow-up*

Patients with ICs were followed up clinically and radiologically every 3 months for the first two years after surgery, every 6 months for the third year after surgery, and annually beginning in the fourth year after surgery. Local tumor recurrence was based on worsening clinical presentation, radiographic changes, and histopathology during secondary procedures during patient follow-up. Local recurrence-free survival (LRFS) was defined as the interval between the date of surgery and the date of diagnosis of the first local recurrence. Similarly, overall survival (OS) was defined as the interval between tumor resection and death from any cause. Observations were censored when patients were tumor free (LRFS analysis) or alive (OS analysis) before April 2022.

*RNA sequencing*

Total RNA was extracted from 40 chordoma tissue samples and 7 nucleus pulposus samples using the RNA isolation kit TRIzol (Invitrogen, USA) following the manufacturer's instructions. RNA sequencing was performed by BGI, and gene expression was quantified by RSEM [27].

*Bioinformatics analysis*

The DESeq2 R package was used to identify differentially expressed lncRNAs between chordoma tissues and nucleus pulposus samples. LncRNAs whose expression was up- or down-regulated according to adjusted *p* values in the chordoma cohort were visualized using the Volcano R package. The "c2.cp.kegg.v7.4", "c5.go.mf.v7.4", "c5.go.bp.v7.4" and "c5.go.cc.v7.4" gene sets for running GSVA were obtained from The Molecular Signatures Database (MSigDB; Fig. http://www.gsea-msigd.org/gsea/login.jsp). A $p$ value < 0.05 indicated statistical significance.

*Cell culture*

The human chordoma cell lines UM-Chor1 and U-CH1 were obtained from the Institute of Basic Medicine, Chinese Academy of Medical Sciences (Beijing, China). UM-Chor1 and U-CH1 cells were cultured in DMEM (Gibco, Pittsburgh, PA, USA) with 10% fetal bovine serum (HyClone, Logan, UT, USA), 100 U/mL penicillin, and 100 μg/mL streptomycin. The cells were cultivated in a humidified atmosphere containing 5% $CO_2$ at 37°C. The authenticity of the cell lines was confirmed through short tandem repeat analysis. DAPI staining was employed to ensure the absence of mycoplasma contamination in all the cell lines. In this study, the passages of all the cell lines used were limited to twenty after receipt or resuscitation.

*RNA fluorescence in situ hybridization (FISH)*

FISH analysis was conducted using the FISH Tag™ RNA Multicolor Kit (Invitrogen, USA) following the manufacturer's protocol. Oligonucleotide probes specific for the lnc-GLYATL2-2 sequence were synthesized by GeneChem (Shanghai, China). Images were captured using a high-precision imaging system consisting of an ECLIPSE Ts2 fluorescence microscope (Nikon, Japan).

*Construction and transfection of lentiviral vectors*

Lentiviral vectors were synthesized by GeneChem (Shanghai, China) to achieve stable overexpression of lnc-GLYATL2-2, ELAVL1, and their respective negative controls. Additionally, Gene-Chem provided lentiviral vectors for RNAi-mediated knockdown of these target genes. The specific RNAi sequences utilized in this study can be found in Supplementary Table 1.

*RNA extraction and quantitative real-time PCR (RT-qPCR)*

Total RNA was extracted following the manufacturer's instructions utilizing a RNeasy Kit (Qiagen). Reverse transcription was performed using the SuperScript™ III CellsDirect™ cDNA Synthesis Kit (Invitrogen). RT-qPCR analysis was conducted using TB Green® Premix Ex Taq™ (Tli RNaseH Plus) (TaKaRa). The relative mRNA or lncRNA expression levels were determined using the ΔΔCt method and normalized to the expression of GAPDH. The primers used were designed using the Primer3Plus online tool and are listed in Supplementary Table 2.

*Western blotting*

Chordoma cells from various groups were lysed using RIPA buffer with 1% protease and phosphatase inhibitors (Beyotime Biotechnology,

Beijing, China). The resulting protein samples were quantified and denatured, separated via SDS-PAGE and subsequently transferred onto PVDF membranes. These membranes were subsequently subjected to overnight incubation at 4°C with a primary antibody specific for the target protein. Following thorough washing to remove excess primary antibody, the membranes were incubated with the appropriate secondary antibody at room temperature for 1 hour. Visualization of the protein bands was achieved using an enhanced chemiluminescence (ECL) kit (Beyotime Biotechnology, Beijing, China) and a chemiluminescence imaging system (Tanon, Shanghai, China). A comprehensive list of the antibodies used in this study can be found in Supplementary Table 3.

*Protein stability assessment*

Chordoma cells from different experimental groups were pretreated with 50 μM of the proteasome inhibitor MG132 (Sigma-Aldrich). Following protein extraction, the target proteins were detected through western blotting analysis. Moreover, chordoma cells were exposed to 50 μg/ml cycloheximide (Sigma-Aldrich), an inhibitor of neoprotein synthesis, and subsequently lysed at 0 h, 2 h, 4 h, 8 h, and 12 h for assessment of protein half-life via western blotting.

*RNA pulldown assay*

The RNA pulldown assay was conducted using the Pierce™ Magnetic RNA-protein pulldown kit (Thermo Fisher Scientific, USA) according to the manufacturer's guidelines. In summary, lysates derived from chordoma cells were incubated with biotinylated probes specific for lnc-GLYATL2-2 and the PD-L1 mRNA 3'UTR with antisense or mutant sequences. The levels of the interacting proteins were subsequently validated through western blot analysis.

*RNA immunoprecipitation (RIP) assay*

An EZ-Magna RIP kit (Millipore, Darmstadt, Germany) was used to perform an RNA immunoprecipitation (RIP) assay following the manufacturer's instructions. In brief, chordoma cells were lysed using RIP buffer and then incubated with magnetic beads conjugated to anti-ELAVL1 and anti-PD-L1 antibodies. The expression levels of lnc-GLYATL2-2, PD-L1 and the PD-L1 mRNA 3'UTR were measured using RT-qPCR.

*RNA stability assay*

Chordoma cells with ELAVL1 knockdown or overexpression were subjected to treatment with 5 μg/mL actinomycin D (Sigma-Aldrich) for 2, 4, 6, 8, or 10 hours. Total RNA was extracted from the chordoma cells, and the expression levels of PD-L1 were determined through qPCR analysis to calculate the turnover rate and half-life ($t_{1/2}$) of the RNA.

*Immunofluorescence (IF) assay*

For an immunofluorescence (IF) staining assay of chordoma cells, the growth status of well-cultured tumor cells was initially evaluated by performing fixation, permeabilization, and antigen blocking procedures. Subsequently, the cells were subjected to an overnight incubation at 4°C with the primary antibody. Next, a secondary antibody conjugated with a fluorescent probe was introduced and allowed to incubate at room temperature for 1 hour. For visualization of the cell nuclei, DAPI dye (Abcam) was used as a staining agent. Ultimately, the experimental outcomes were visualized through the use of an Eclipse Ts2 fluorescence microscope (Nikon, Japan).

*Immunohistochemistry (IHC)*

Immunohistochemical staining of chordoma specimens was performed as previously described [28]. Tumor sections were labeled and stained with primary antibodies against PD-1, PD-L1, CD8, CD4, and Foxp3 (1:200; Abcam, Cambridge, UK), and the staining results were photographed and recorded using a DM1000 light microscope (Leica).

*Semiquantitative analysis*

After we ensured the confidentiality of the patient's clinical data, immunoreactivity was assessed and semiquantitatively scored by two expert pathologists. As mentioned earlier [25], PD-L1 expression was assessed by the staining scale and percentage of positively stained cells. The staining scales used were as follows: none, 0; weak, 1; moderate, 2; and intensive, 3. The percentage of immune-positive cells was scored as follows: 0%, 0; 1-10%, 1; 11-50%, 2;

51-80%, 3; and 81-100%, 4. The immunohistochemical score was calculated as the product of two grades (percentage of immunopositive cells × staining scale), and positive expression was defined as a score ≥ 4 [29, 30]. The infiltration degree of TILs was assessed as previously described (0), rare/few (1), moderate (2), or prominent (3). Chordoma samples were divided into negative staining (score 0-1) and positive staining (score 2-3) groups [31, 32].

*Quantitative evaluation*

Ten different high-power fields were examined in each section to assess TILs quantitatively for each tumor tissue. The numbers of $CD4^+$, $CD8^+$, $Foxp3^+$, and $PD\text{-}1^+$ TILs in the corresponding pathological sections were counted five times for each tumor tissue sample and recalculated when significant differences emerged. Eventually, the number of cells with positive staining per unit area ($mm^2$) was computed as the average density of infiltrating cells [33].

*Statistical analysis*

The statistical analysis for this study was performed with R 4.2.1 and Prism 9.0 software. Comparisons between two independent samples and variances among multiple samples were obtained by t tests and one-way ANOVA. The Wilcoxon test was used for the statistical analysis of nonparametric data. Pearson correlation was used to calculate the relevance between two or more groups. Kaplan-Meier curves were used to evaluate the survival rates of diverse patient groups.

## Result

*Identification of lnc-GLYATL2-2 as a potential regulator of PD-L1 expression in ICs*

We analyzed the RNA-seq data of 40 ICs and 7 normal control tissues and found that the expression of acquired lncRNAs was correlated with the expression of the TIL markers CD4, CD8, and Foxp3 and the immune checkpoints PD-1 and PD-L1. Among them, 13 lncRNAs were negatively correlated with CD8 expression and positively correlated with CD4, Foxp3, PD-1 and PD-L1 expression (**Figure 1A**). Moreover, differential gene analysis of RNA-seq data from chordoma and normal tissues revealed that among the above 13 lncRNAs, only lnc-GLYATL2-2 was upregulated in chordoma tissues (**Figure 1B**, **1C**). GSEA indicated that there was enrichment of the PD-1/PD-L1 signaling pathway in the lnc-GLYATL2-2 high-expression group in chordoma (**Figure 1D**, **1E**). GO and KEGG analyses showed that lnc-GLYATL2-2 was correlated with immunomodulatory function (**Figure 1F**). Moreover, we assessed lnc-GLYATL2-2 expression in our 96 clinical chordoma tissues by qPCR and found that lnc-GLYATL2-2 had higher expression than that in the normal control tissues ($P < 0.001$; **Figure 1G**). According to the RNA-seq data, the expression of lnc-GLYATL2-2 and PD-L1 was strongly positively correlated ($r=0.718$, $P < 0.001$; **Figure 1H**). Furthermore, the expression of immune modulatory molecules, including cytokines and their receptors, plays a crucial role in regulating the tumor microenvironment. Therefore, based on our RNA-seq results, we further investigated the relationships between chemokine, chemokine receptor, immune stimulatory molecule, immune inhibitory molecule, and lnc-GLYATL2-2 expression in intracranial chordomas. A detailed list of these immunomolecules was obtained from the TISIDB database (http://cis.hku.hk/TISIDB/index.php). Correlation analysis revealed a moderate positive correlation between lnc-GLYATL2-2 and chemokine receptors as well as immune inhibitory molecules. However, the correlation between chemokines and immune stimulatory molecules appeared to be relatively weak (Supplementary Figure 1A-D). Additionally, we investigated PD-L1 expression in chordoma patients by immunohistochemical staining (**Figure 2A**) and found that the PD-L1-positive group exhibited higher lnc-GLYATL2-2 expression than the PD-L1-negative group ($P < 0.001$; **Figure 1I**). Taken together, the above results showed that lnc-GLYATL2-2 was upregulated in ICs and that there was an apparent positive correlation between lnc-GLYATL2-2 and PD-L1 expression, suggesting that lnc-GLYATL2-2 may act as a key regulator of PD-L1 expression in ICs.

*Correlations among lnc-GLYATL2-2 and PD-L1 expression, microenvironmental TILs, and clinicopathological features in ICs*

The expression level of lnc-GLYATL2-2 in ICs was strongly correlated with enhanced tumor aggressiveness ($P=0.002$; **Table 1**). In a cohort

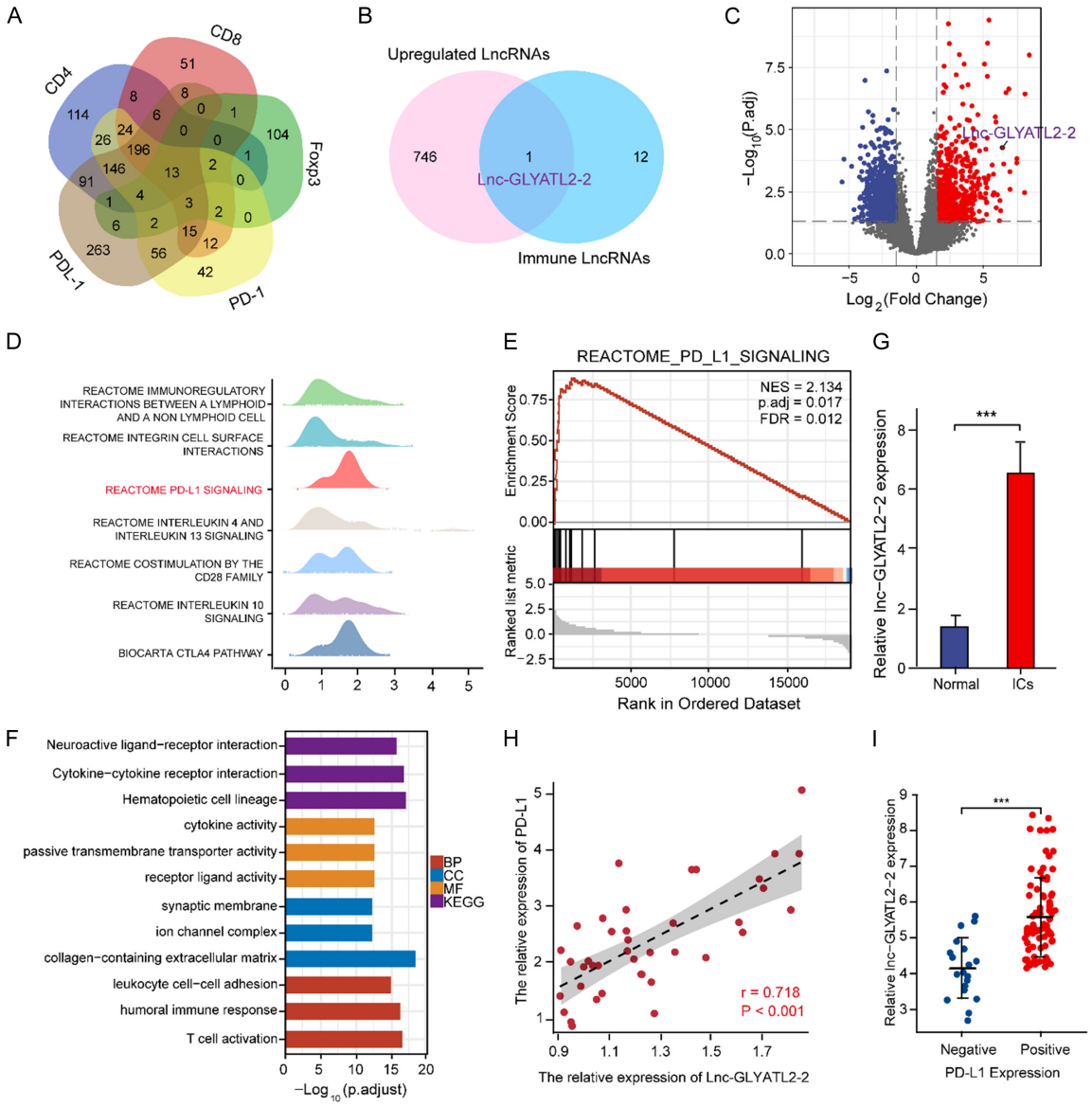


**Figure 1.** Identification of lnc-GLYATL2-2 as a potential regulator of PD-L1 expression in ICs. (A) LncRNAs correlated with CD4, CD8, Foxp3, PD-1 and PD-L1 expression levels in ICs. (B) The LncRNAs are upregulated in ICs and associated with immune markers. (C) Volcano plots showing the differentially expressed lncRNAs between ICs and normal control tissues. (D, E) GSEA showing signaling pathways enriched in the lnc-GLYATL2-2 high expression group of ICs (D), GSEA analysis showing the enrichment of PD-L1 signaling in high lnc-GLYATL2-2 expression group (E). (F) GO and KEGG analysis in the lnc-GLYATL2-2 high expression group of ICs. (G) RT-qPCR assay detecting lnc-GLYATL2-2 expression levels in ICs and normal control tissues. (H) RNA-seq data of ICs showing expressed correlation between PD-L1 and lnc-GLYATL2-2. (I) Statistics analysis of lnc-GLYATL2-2 expression in different PD-L1 expression patterns of ICs. All data are presented as the mean ± SD (three independent experiments). *P < 0.05; **P < 0.01; ***P < 0.001; ns, no significance.

of chordoma patients, PD-L1 was identified in 80.2% (77/96) of the tumor tissues by immunohistochemical staining. Additionally, a greater frequency of tumor invasion was present in patients with PD-L1-positive chordomas (P=0.012; **Table 1**). We evaluated TILs in 96 IC samples by HE staining; 18 patients had negative results for TILs, and the remaining 78 patients were positive for TILs. Subsequently, we assayed the PD-1 expression of TILs in 96 tumor specimens. The mean PD-1$^+$ TIL density was 242.3 cells/mm$^2$. A high density of PD-1$^+$

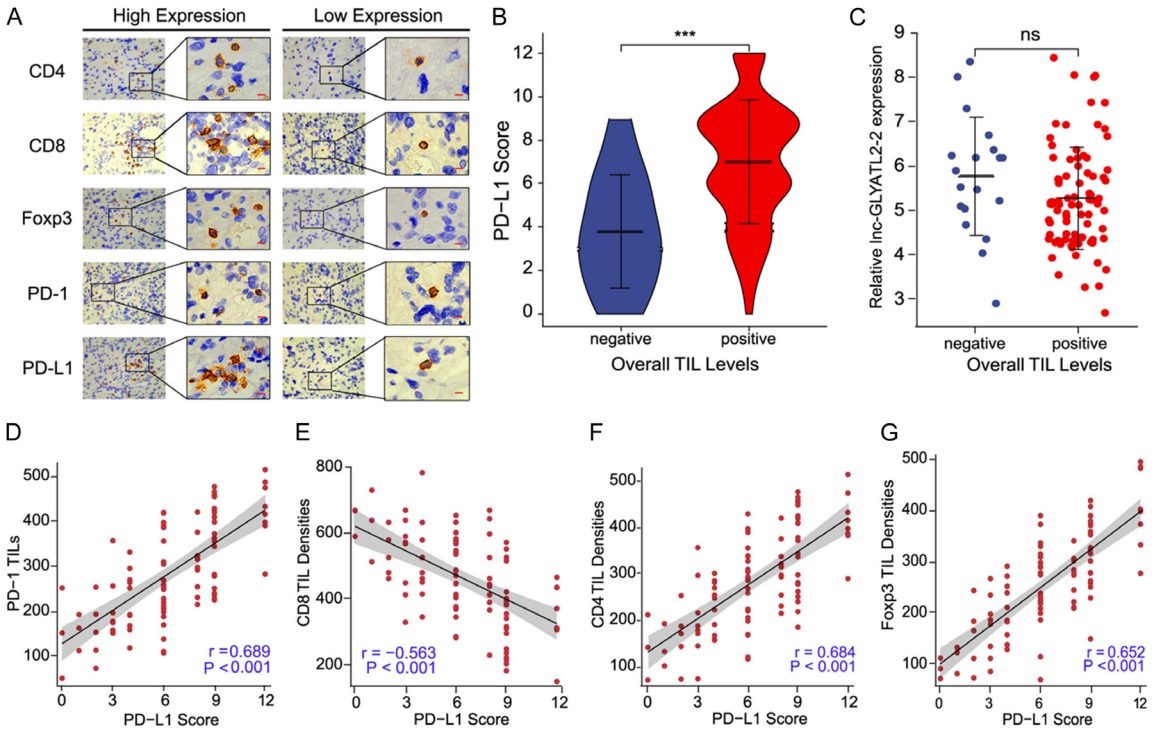


**Figure 2.** The correlation between the lnc-GLYATL2-2/PD-L1 axis and TIL subsets in ICs. (A) Immunohistochemical staining of CD4, CD8, Foxp3, PD-1 and PD-L1 in ICs. Scale bar =50 μm. (B) Association between PD-L1 scores and overall TIL levels. (C) The relationship between lnc-GLYATL2-2 expression and overall TIL levels. (D-G) Correlation between PD-L1 scores and TIL subsets: PD-1$^+$ TILs (D), CD8$^+$ TILs (E), CD4$^+$ TILs (F), and Foxp3$^+$ TILs (G). Data are shown as the mean ± SD (three independent experiments). *P < 0.05; **P < 0.01; ***P < 0.001; ns, no significance.

TILs was associated with a high degree of tumor infiltration (P < 0.001; **Table 1**). To explore the fractional composition of the infiltrating lymphocytes in the immune microenvironment of chordoma tumors, we detected CD4$^+$, CD8$^+$, and Foxp3$^+$ TILs in all chordoma specimens. The mean densities of CD4$^+$, CD8$^+$, and Foxp3$^+$ TILs were 263.1, 483.7, and 218.3 cells/mm$^2$, respectively. However, there were no significant correlations between the densities of CD4$^+$, CD8$^+$, or Foxp3$^+$ TILs and the clinicopathological features of chordoma patients.

*Relationship between the lnc-GLYATL2-2/PD-L1 axis and microenvironmental TIL subsets in ICs*

In patients with ICs, we found that positive PD-L1 expression correlated with a high number of TILs (**Figure 2B**). However, there was no appreciable correlation between the expression of lnc-GLYATL2-2 and the degree of TIL infiltration in the immune microenvironment of chordoma (**Figure 2C**). In addition, we investigated the correlation between PD-1$^+$, CD4$^+$, CD8$^+$ and Foxp3$^+$ TILs and PD-L1 expression in the immune microenvironment of chordoma. We observed that all four types of TILs exhibited a significant positive or negative correlation with the expression of PD-L1 (**Figure 2D-G**). Furthermore, we performed a statistical analysis of the extent of infiltration of CD8$^+$, CD4$^+$, and FOXP3$^+$ TILs in chordoma specimens using immunohistochemical staining based on the differential expression of lnc-GLYATL2-2. Analysis revealed a significant increase in the number of CD4$^+$ and Foxp3$^+$ T cells in the lnc-GLYATL2-2 high-expression group, while a greater degree of infiltration of CD8$^+$ T cells was observed in the lnc-GLYATL2-2 low-expression group (Supplementary Figure 2A-C).

*Clinical importance of the lnc-GLYATL2-2/PD-L1 axis and TIL subtypes in IC patients*

During the follow-up of a cohort of 96 IC patients, tumor progression was observed in 52 patients (54.2%), with LRFS rates of 88.5% (85/96) at 1 year and 38.5% (37/96) at 3 years. Over the follow-up period, 45 patients died

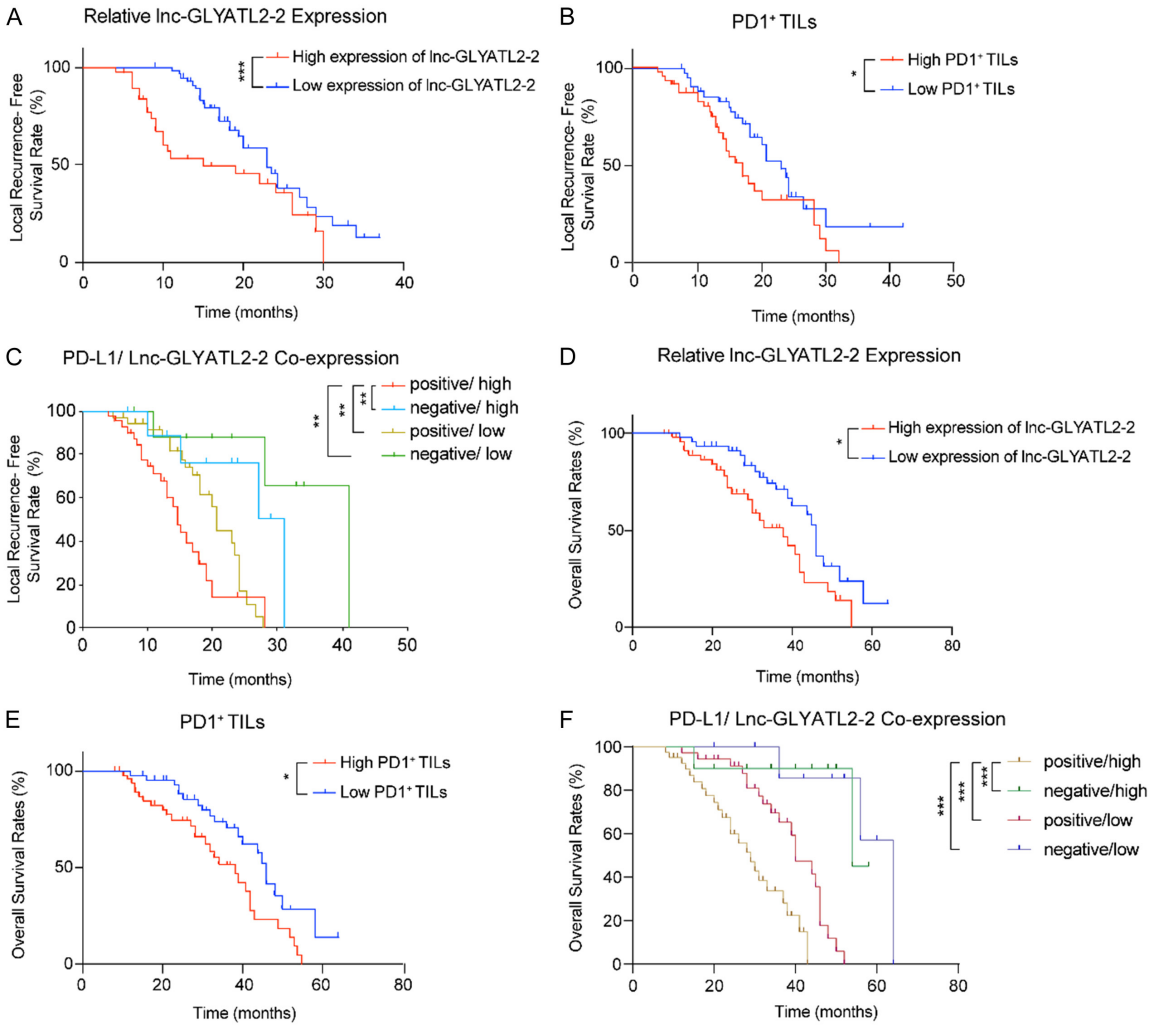


**Figure 3.** Survival impact of lnc-GLYATL2-2/PD-L1 axis in ICs. (A-F) Kaplan-Meier analysis of LRFS in different ICs groups. (A-C) Classification by lnc-GLYATL2-2 expression levels (A), PD-1$^+$ TIL densities (B), lnc-GLYATL2-2 and PD-L1 co-expression (C). Kaplan-Meier analysis of OS in different ICs groups. (D-F) Category by lnc-GLYATL2-2 expression levels (D), PD-1$^+$ TIL densities (E), lnc-GLYATL2-2 and PD-L1 co-expression (F). *P < 0.05; **P < 0.01; ***P < 0.001; ns, no significance.

(46.9%), with OS rates of 100, 76.0, and 42.7% at 1, 3, and 5 years, respectively. The mean LRFS and OS of patients in this cohort were 24.1 months (2-42 months) and 44.3 months (13-68 months), respectively.

Based on RNA-seq data from chordoma specimens, we ranked the specimens in descending order of their lnc-GLYATL2-2 expression and obtained the median expression value of lnc-GLYATL2-2. Chordoma samples with expression levels exceeding this median were classified into the lnc-GLYATL2-2 high-expression group, while samples with expression levels below the median were assigned to the low-expression group. Similarly, PD-1$^+$ TIL density was also estimated to investigate survival time in a cohort of patients with chordoma. Patients were divided into high- and low-expression groups according to the median values. A high expression level of lnc-GLYATL2-2 and a high PD-1$^+$ TIL density indicated poor LRFS and OS in IC patients (**Figure 3A**, **3B**, **3D**, **3E**). Kaplan-Meier analysis demonstrated that PD-L1 and lnc-GLYATL2-2 coexpression levels are correlated with patient survival time. Positive expression of PD-L1 and high expression of lnc-GLYATL2-2 indicated a shorter period of tumor progression or recurrence than did the other groups (**Figure 3C**). Moreover, multivariate Cox regression analysis revealed that the degree of infiltration of PD-1$^+$ TILs and the lnc-GLYATL2-2/CD8 ratio could be

**Table 2.** Univariate and multivariate Cox regression analysis of prognostic parameters for LRFS of ICs patients

| Factors | Categories | Univariate analysis | | Multivariate analysis | |
|---|---|---|---|---|---|
| | | $\chi^2$ | *p* values | *p* values | HR (95% CI) |
| Sex | Male/female | 0.833 | 0.528 | | |
| Age | ≤ 50/> 50 | 0.018 | 0.922 | | |
| Location | Superior/middle/inferior clivus | 0.627 | 0.793 | | |
| Tumor size | ≤ 4 cm/> 4 cm | 0.548 | 0.494 | | |
| Invasion condition | Yes/no | 12.371 | 0.003 | 0.065 | 2.163 (0.831-3.585) |
| Preoperative recurrence | Yes/no | 2.473 | 0.206 | | |
| Rate of resection | > 90%/≤ 90% | 10.327 | 0.005 | 0.373 | 0.726 (0.437-1.677) |
| Histopathology | Conventional/chondroid | 0.117 | 0.780 | | |
| Chordoma PD-L1 expression | Positive/negative | 2.132 | 0.094 | | |
| Chordoma lnc-GLYATL2-2 expression | High/low | 11.346 | 0.001 | 0.572 | 1.591 (0.792-2.605) |
| PD-L1/lnc-GLYATL2-2 co-expression | Negative/low | 11.585 | 0.008 | 0.769 | 1.803 (0.414-3.072) |
| | Negative/high | | | | |
| | Positive/low | | | | |
| | Positive/high | | | | |
| PD-1$^+$ TILs | High/low | 12.302 | < 0.001 | 0.028 | 0.305 (0.184-0.798) |
| Lnc-GLYATL2-2/CD8 ratio | High/low | 15.086 | < 0.001 | 0.020 | 0.270 (0.197-0.571) |

**Table 3.** Univariate and multivariate Cox regression analysis of prognostic parameters for OS of ICs patients

| Factors | Categories | Univariate analysis | | Multivariate analysis | |
|---|---|---|---|---|---|
| | | $\chi^2$ | *p* values | *p* values | HR (95% CI) |
| Sex | Male/female | 0.274 | 0.883 | | |
| Age | ≤ 50/> 50 | 0.566 | 0.752 | | |
| Location | Superior/middle/inferior clivus | 3.723 | 0.097 | | |
| Tumor size | ≤ 4 cm/> 4 cm | 0.061 | 0.596 | | |
| Invasion condition | Yes/no | 8.256 | 0.034 | 0.193 | 1.627 (0.655-3.276) |
| Preoperative recurrence | Yes/no | 0.264 | 0.360 | | |
| Rate of resection | > 90%/≤ 90% | 0.393 | 0.463 | | |
| Histopathology | Conventional/chondroid | 2.465 | 0.267 | | |
| Chordoma PD-L1 expression | Positive/negative | 1.389 | 0.010 | 0.637 | 0.792 (0.487-1.552) |
| Chordoma lnc-GLYATL2-2 expression | High/low | 5.435 | 0.028 | 0.475 | 1.839 (0.764-3.473) |
| PD-L1/lnc-GLYATL2-2 co-expression | Negative/low | 7.772 | 0.042 | 0.072 | 2.138 (0.592-5.094) |
| | Negative/high | | | | |
| | Positive/low | | | | |
| | Positive/high | | | | |
| PD-1$^+$ TILs | High/low | 5.792 | 0.010 | 0.032 | 1.735 (1.025-2.360) |
| Lnc-GLYATL2-2/CD8 ratio | High/low | 8.519 | 0.006 | 0.018 | 2.415 (1.438-3.772) |

regarded as independent predictors of LRFS (**Table 2**). Survival analysis revealed that high lnc-GLYATL2-2 expression and a high degree of infiltration of PD-1$^+$ TILs were associated with shorter OS. Similar to the LRFS analysis, PD-L1 and lnc-GLYATL2-2 coexpression was linked to a greater risk of death in patients with these features than in patients in the other groups (**Figure 3F**). A high degree of infiltration of PD-1$^+$ TILs and a high lnc-GLYATL2-2/CD8 ratio portended a worse survival prognosis according to the conclusions of a multifactorial Cox regression analysis (**Table 3**).

*Identification of ELAVL1 as a target of lnc-GLYATL2-2 in chordoma cells*

Based on the results of RNA-seq analysis of clinical specimens of ICs, we discovered a strong positive correlation between the expres-

sion of lnc-GLYATL2-2 and PD-L1 at the transcriptional level. Therefore, we further investigated the regulatory effect of lnc-GLYATL2-2 on PD-L1 expression. Initially, using the lncTar database (https://www.cuilab.cn/lnctar), we found that lnc-GLYATL2-2 does not directly interact with PD-L1 mRNA. Thus, we hypothesized that lnc-GLYATL2-2 may indirectly participate in the regulation of PD-L1 expression through binding to RBPs. The analytical results obtained from the ENCORI/StarBase (Encyclopedia of RNA Interactomes) (https://rnasysu.com/encori/) revealed that both lnc-GLYATL2-2 and PD-L1 mRNA can bind to ELAVL1 (**Figure 4A**). ELAVL1 is a classic RBP known to bind to the 3'UTR of mature mRNA, maintaining its stability and promoting transcription. Therefore, we examined the binding capacity of ELAVL1 to the PD-L1 mRNA 3'UTR. Predictions acquired from the RBPsuite database (http://www.csbio.sjtu.edu.cn/bioinf/RBPsuite/) revealed specific binding sites between ELAVL1 and the PD-L1 mRNA 3'UTR (Supplementary Table 4). To further confirm the interaction between ELAVL1 and the PD-L1 mRNA 3'UTR, we performed RNA pulldown and RIP assays in the UM-Chor1 cell line. Analysis indicated that the PD-L1 mRNA 3'UTR probe exhibited affinity for the ELAVL1 protein, and anti-ELAVL1 treatment led to enrichment of the PD-L1 mRNA 3'UTR (**Figure 4B**, **4D**, **4E**). Similarly, the interaction between ELAVL1 and lnc-GLYATL2-2 was also validated (**Figure 4C**, **4F**, **4G**).

*Lnc-GLYATL2-2 enhances the stability of PD-L1 mRNA by increasing the nuclear export of ELAVL1*

To further study whether ELAVL1 is involved in the regulation of PD-L1 mRNA expression by lnc-GLYATL2-2, we examined the expression of PD-L1 at the mRNA and protein levels using qPCR and western blotting. The results showed that overexpression of lnc-GLYATL2-2 upregulated PD-L1 at both the transcriptional and translational levels, and these effects were significantly reversed by silencing ELAVL1 (**Figure 4H-J**). To investigate the possible mechanism through which lnc-GLYATL2-2 and ELAVL1 regulate PD-L1 expression, we examined the distribution of ELAVL1 in cells with overexpression or knockdown of lnc-GLYATL2-2 using a WB assay. The results demonstrated that knockdown of lnc-GLYATL2-2 significantly decreased the cytoplasmic level of ELAVL1, while overexpression of lnc-GLYATL2-2 significantly increased the transfer of ELAVL1 from the nucleus to the cytoplasm (**Figure 4K**, **4L**). Additionally, immunofluorescence experiments confirmed that under lnc-GLYATL2-2 knockdown conditions, ELAVL1 was localized mainly to the nucleus, while overexpression of lnc-GLYATL2-2 significantly increased the cytoplasmic distribution of ELAVL1 (**Figure 4M**). Moreover, a RIP assay confirmed that under conditions of lnc-GLYATL2-2 overexpression, anti-ELAVL1 treatment contributed to greater enrichment of the PD-L1 mRNA 3'UTR, while silencing lnc-GLYATL2-2 rescued these changes (**Figure 4N**, **4O**). Furthermore, as ELAVL1 primarily binds to the PD-L1 mRNA 3'UTR to maintain its stability, RNA stability analysis was further conducted using actinomycin D. Overexpression of lnc-GLYATL2-2 significantly prolonged the half-life of PD-L1 mRNA, while knockdown of lnc-GLYATL2-2 decreased the stability of PD-L1 mRNA, leading to a significantly shortened half-life (**Figure 4P**, **4Q**). In summary, these experimental findings illustrate that the upregulation of lnc-GLYATL2-2 leads to increased nuclear export of ELAVL1, promoting its cytoplasmic distribution and interaction with the PD-L1 mRNA 3'UTR to maintain the stability of PD-L1 mRNA and upregulate PD-L1 expression.

*Lnc-GLYATL2-2 enhances PD-L1 stability by directly binding ICs*

LncRNAs often interact with proteins due to their complex molecular structure, thereby influencing their functions. Based on the predictions from the CatRAPID database, we found that lnc-GLYATL2-2 can directly bind to the PD-L1 protein (**Figure 5A**). To validate this prediction, we first studied the cellular localization of lnc-GLYATL2-2. FISH revealed that lnc-GLYATL2-2 is distributed mainly in the cytoplasm of the chordoma cell lines UM-Chor1 and U-CH1 (**Figure 5B**). To further confirm the interaction between lnc-GLYATL2-2 and PD-L1, we performed RNA pulldown and RIP assays with UM-Chor1 and U-CH1 cells. Analysis revealed that the lnc-GLYATL2-2 probe exhibited affinity for the PD-L1 protein, and anti-PD-L1 treatment resulted in the enrichment of lnc-GLYATL2-2 (**Figure 5C-H**). Based on these results, we speculate that the direct binding of

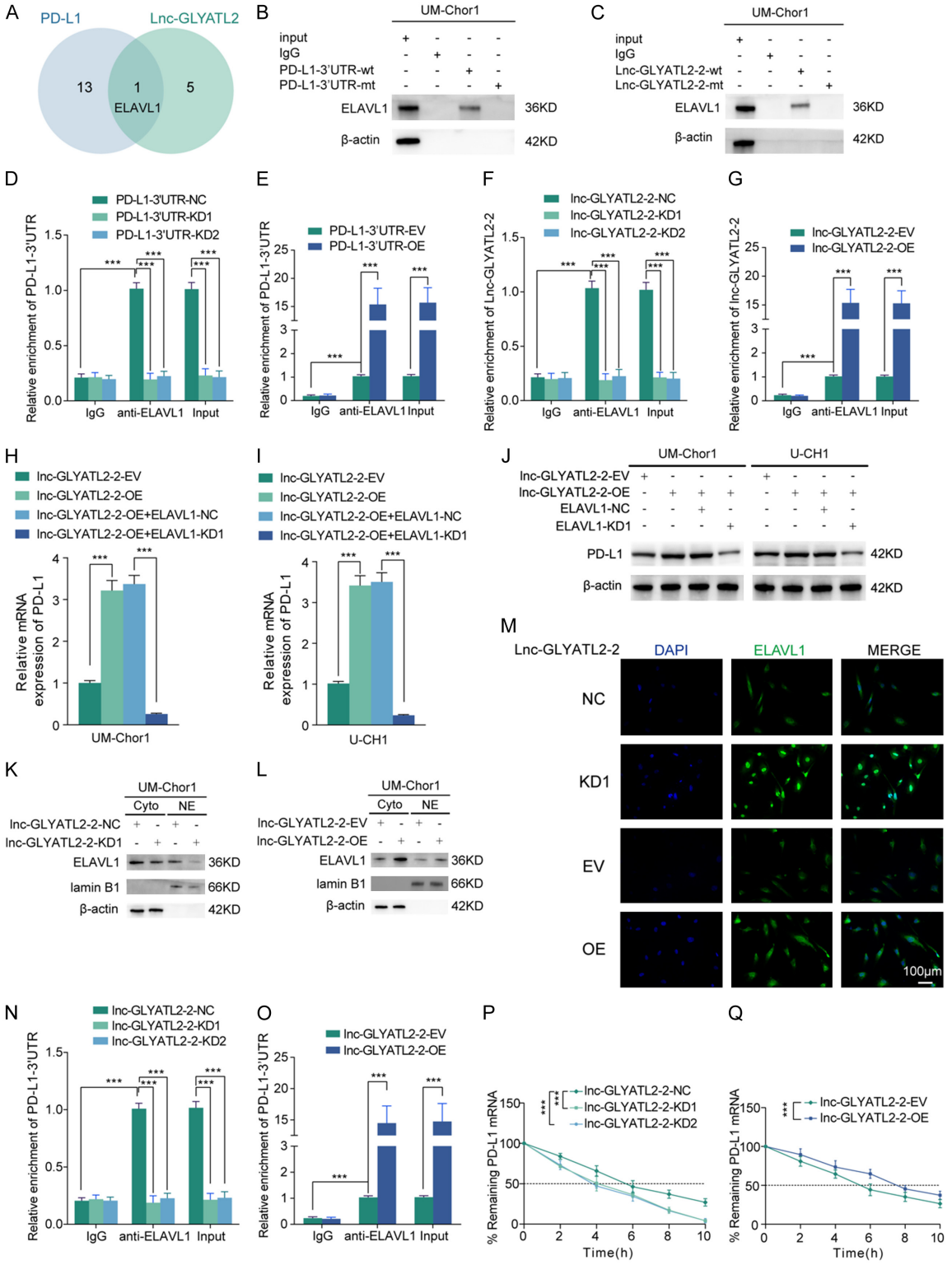


**Figure 4.** The lnc-GLYATL2-2 interacts with ELAVL1 to mediate enhanced stability of PD-L1 mRNA and facilitates its expression. (A) Venn diagram illustrating the RBPs (RNA-binding proteins) that can interact with both PD-L1 and lnc-GLYATL2-2. (B, C) RNA pull-down assays in UM-Chor1 displayed the PD-L1-3'UTR probe (B) and lnc-GLYATL2-2probe (C) pulled down ELAVL1 proteins. (D, E) RIP assays showed anti-ELAVL1 treatment leaded to PD-L1-3'UTR enrichment in lnc-GLYATL2-2-silenced UM-Chor1 (D) and lnc-GLYATL2-2-overexpressed UM-Chor1 (E). (F, G) RIP assays showed anti-ELAVL1 treatment leaded to lnc-GLYATL2-2 enrichment in PD-L1-3'UTR-silenced UM-Chor1 (F) and PD-L1-3'UTR-overexpressed UM-Chor1 (G). (H, I) qPCR assays of the transcriptional levels of PD-L1 in lnc-GLYATL2-

2-overexpressed UM-Chor1 (H) as well as lnc-GLYATL2-2-overexpressed U-CH1 (I) after ELAVL1 silencing. (J) Western blotting showed the protein level change of PD-L1 after lnc-GLYATL2-2 overexpression with ELAVL1 knockdown in UM-Chor1. (K, L) ELAVL1 expression in cytoplasm and nuclei of lnc-GLYATL2-2-silenced UM-Chor1 (K) and lnc-GLYATL2-2-overexpressed UM-Chor1 (L). (M) Representative images of IF staining assays illustrated the subcellular distribution of ELAVL1 in lnc-GLYATL2-2-silenced and lnc-GLYATL2-2-overexpressed UM-Chor1. Scale bar =100 μm. (N, O) RIP assays showed anti-ELAVL1 treatment leaded to PD-L1-3'UTR enrichment in lnc-GLYATL2-2-silenced UM-Chor1 (N) and lnc-GLYATL2-2-overexpressed UM-Chor1 (O). (P, Q) RNA stability assays showing the half-life of PD-L1 in lnc-GLYATL2-2-silenced (P) or overexpressed (Q) UM-Chor1 followed by actinomycin D treatment. Data are shown as the mean ± SD (three independent experiments). *P < 0.05; **P < 0.01; ***P < 0.001; ns, no significance.

lnc-GLYATL2-2 to PD-L1 may affect the protein stability of PD-L1. Next, we treated chordoma cell lines with the proteasome inhibitor MG132 and found that MG132 treatment notably rescued the downregulation of PD-L1 expression caused by lnc-GLYATL2-2 knockdown, while in cells with lnc-GLYATL2-2 upregulation, MG132 treatment further resulted in PD-L1 overexpression (**Figure 5I**, **5J**). Additionally, a CHX experiment was used to analyze the protein stability of PD-L1. Overexpression of lnc-GLYATL2-2 significantly prolonged the half-life of the PD-L1 protein, while lnc-GLYATL2-2 knockdown led to a shortened half-life of the PD-L1 protein (**Figure 5K-N**). Immunofluorescence assays were also conducted to confirm that overexpression of lnc-GLYATL2-2 significantly upregulated the membrane expression of PD-L1 in chordoma cells, while lnc-GLYATL2-2 knockdown generated an apparent reduction in PD-L1 expression (**Figure 5O**, **5P**). In conclusion, our research findings suggest that lnc-GLYATL2-2 can directly bind to the PD-L1 protein and upregulate the expression of PD-L1 in chordoma cells by maintaining its stability.

*Lnc-GLYATL2-2 could be a predictor for immunotherapy efficacy in ICs*

Immunotherapy may have a more sustained antitumor effect than conventional chemotherapy and radiotherapy [34]. However, during some clinical trials, investigators have observed insensitivity to anti-PD therapy in some patients with malignancies [35]. Therefore, predicting whether a patient responds to anti-PD treatment is essential for the rational use of immune checkpoint blockers. The tumor immune dysfunction and exclusion (TIDE) algorithm can accurately predict the response to immunotherapy [36]. We divided the patient cohort into high- and low-expression groups according to the expression level of lnc-GLYATL2-2. According to the TIDE algorithm, higher TIDE scores were observed in the high-lnc-GLYATL2-2 expression subgroup (P < 0.001; **Figure 6A**), suggesting that low lnc-GLYATL2-2 expression may mediate susceptibility to immunotherapy in patients with chordoma. In contrast, high expression of lnc-GLYATL2-2 indicates the potential for immune checkpoint inhibitor therapy escape. Additionally, based on our comprehensive analysis of clinical data from a well-characterized chordoma cohort, we observed a significant correlation between high expression of Lnc-GLYATL2-2 and increased tumor invasiveness. To further validate these findings, we conducted Transwell assays to detect the invasion and migration of chordoma cell lines in vitro. The results revealed a significant reduction in cell invasion and migration following the knockdown of lnc-GLYATL2-2 (Supplementary Figure 3A-D). These findings provide valuable evidence supporting the clinical diagnostic and therapeutic potential of lnc-GLYATL2-2 in treating ICs.

## Discussion

In this study, we found that high expression of lnc-GLYATL2-2 in ICs correlated with worse LRFS and OS. Additionally, patients with pathological features consistent with PD-L1 and lnc-GLYATL2-2 coexpression had the most unfavorable prognoses. Furthermore, the findings suggest that the degree of infiltration of PD-1$^+$ TILs and the lnc-GLYATL2-2/CD8 ratio may serve as independent predictors of LRFS and OS in patients with chordoma. These results reveal the expression of the existing immune checkpoint molecules PD-1 and PD-L1 in ICs and, more crucially, raise awareness of novel lncRNA molecules in the diagnosis, treatment and prognosis of ICs and establish a solid theoretical basis for individualized treatment of ICs.

Cancer immunotherapy primarily targets immune checkpoint molecules, such as PD-1, PD-L1 and CTLA4 [37]. Immune checkpoint blockade, a classical regimen of immunothera-

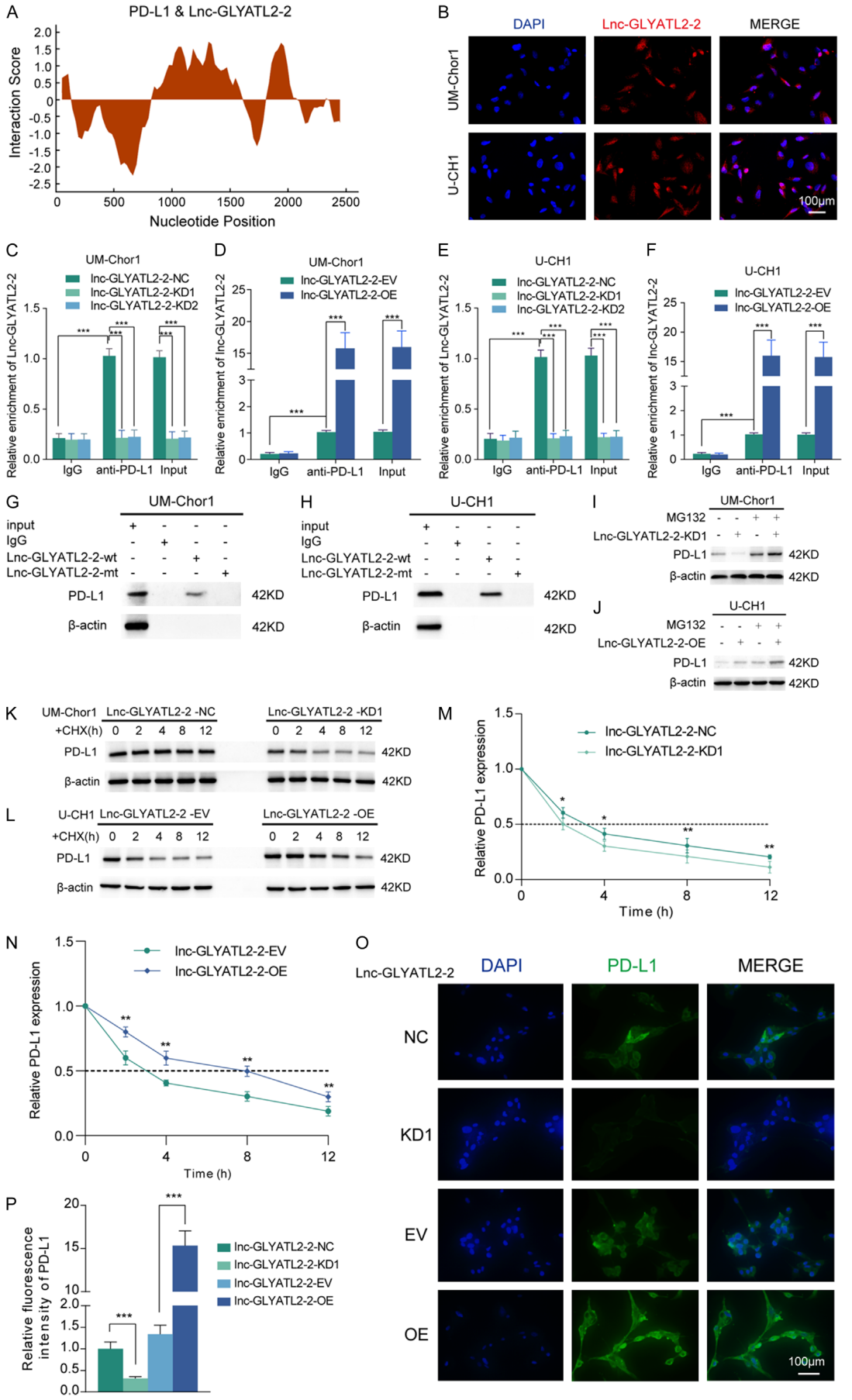
A
PD-L1 & Lnc-GLYATL2-2
Interaction Score
Nucleotide Position
B
DAPI
Lnc-GLYATL2-2
MERGE
UM-Chor1
U-CH1
100μm
C
UM-Chor1
Lnc-GLYATL2-2-NC
Lnc-GLYATL2-2-KD1
Lnc-GLYATL2-2-KD2
Relative enrichment of Lnc-GLYATL2-2
IgG
anti-PD-L1
Input
D
UM-Chor1
Lnc-GLYATL2-2-EV
Lnc-GLYATL2-2-OE
E
U-CH1
F
U-CH1
G
UM-Chor1
input
IgG
Lnc-GLYATL2-2-wt
Lnc-GLYATL2-2-mt
PD-L1
β-actin
42KD
H
U-CH1
I
UM-Chor1
MG132
Lnc-GLYATL2-2-KD1
J
U-CH1
Lnc-GLYATL2-2-OE
K
UM-Chor1
Lnc-GLYATL2-2 -NC
Lnc-GLYATL2-2 -KD1
+CHX(h)
L
U-CH1
Lnc-GLYATL2-2 -EV
Lnc-GLYATL2-2 -OE
M
Relative PD-L1 expression
Time (h)
N
O
Lnc-GLYATL2-2
NC
KD1
EV
OE
P
Relative fluorescence intensity of PD-L1

**Figure 5.** Lnc-GLYATL2-2 interacts with PD-L1 and prevents from degradation. (A) Lnc-GLYATL2-2 binds to PD-L1 proteins via CatRAPID prediction. (B) In situ hybridization detection of lnc-GLYATL2-2 expression in UM-Chor1 and U-CH1. Scale bar =100 μm. (C, D) RIP assays showed anti-PD-L1 treatment leaded to lnc-GLYATL2-2 enrichment in lnc-GLYATL2-2-silenced UM-Chor1 (C) and lnc-GLYATL2-2-overexpressed UM-Chor1 (D). (E, F) RIP assays showed anti-PD-L1 treatment leaded to lnc-GLYATL2-2 enrichment in lnc-GLYATL2-2-silenced U-CH1 (E) and lnc-GLYATL2-2-overexpressed U-CH1 (F). (G, H) RNA pull-down assays in UM-Chor1 (G) and U-CH1 (H) displayed the lnc-GLYATL2-2 probe pulled down PD-L1 proteins. (I, J) The lnc-GLYATL2-2-silenced UM-Chor1 (I) or overexpressed U-CH1 (J) were treated with or without MG-132 (50 μM) for 6 h, and PD-L1 expression was detected by western blotting. (K-N). The lnc-GLYATL2-2-silenced UM-Chor1 (K) or overexpressed U-CH1 (L) were treated with CHX (50 μg/ml) and the expression of PD-L1 protein was detected by western blotting and the half-life time ($t_{1/2}$) was quantitative analysis respectively (M, N). (O, P) Representative images of IF staining assays illustrated the PD-L1 expression in lnc-GLYATL2-2-silenced and lnc-GLYATL2-2-overexpressed UM-Chor1 (O). The relative fluorescence intensity of PD-L1 (P) quantified by Image J. Scale bar =100 μm. Data are shown as the mean ± SD (three independent experiments). *P < 0.05; **P < 0.01; ***P < 0.001; ns, no significance.

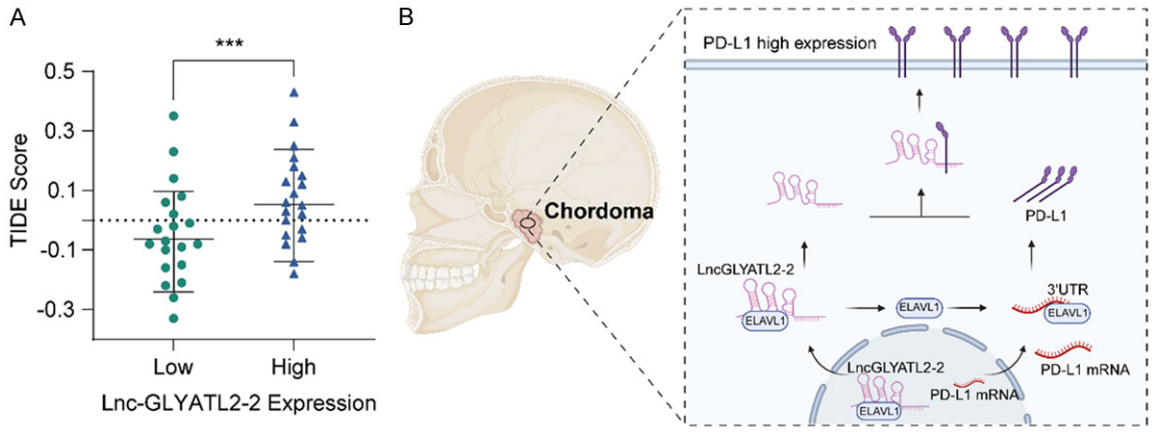


**Figure 6.** Lnc-GLYATL2-2 serves as a crucial biomarker for predicting the efficacy of immunotherapy in ICs. A. The TIDE scores of ICs patients with different lnc-GLYATL2-2 expression levels. B. Schematic diagram showing the lnc-GLYATL2-2 and ELAVL1 synergistically interact to maintain high expression of PD-L1 in ICs. Data are shown as the mean ± SD (three independent experiments). *P < 0.05; **P < 0.01; ***P < 0.001; ns, no significance.

py, is designed to enhance the antitumor activity of killer T cells in the TIME [38]. Immunotherapies, predominantly represented by PD-1/PD-L1 inhibitors, have made substantial breakthroughs in the clinical treatment of various solid tumors [39]. As a result, immunotherapy has become an effective strategy for treating malignancies [40]. An increasing number of studies have demonstrated that several factors in the TIME, including the expression of immune checkpoint molecules, the number of TILs and the presence of neoantigens, may be capable of predicting the responsiveness of patients to immunotherapy [41-43]. Moreover, accumulating evidence indicates that lncRNAs modulate pivotal mechanisms of cancer immunity, ranging from antigen presentation to T-cell depletion [44]. In head and neck squamous cell carcinoma, lncMX1-215 can interact with the acetylase GCN5 H3K27 to prevent PD-L1 expression from leading to tumor resistance to immunotherapy [45]. MALAT1 upregulates PD-L1 expression by adsorbing miR-195 and helps diffuse large B-cell lymphoma and effectuate immune escape [46]. SNHG20 promotes the progression and metastasis of esophageal squamous cell carcinoma by modulating the activity of the ATM-JAK-PD-L1 axis [47]. The lncRNAs mentioned above possess advanced tumor immune signatures and could be employed as diagnostic markers or even therapeutic targets for the TIME [48]. In this study, we verified by bioinformatics analysis and experiments that lnc-GLYATL2-2 was upregulated in ICs and positively regulated PD-L1 expression in tumor cells. In addition, GSEA of RNA-seq data suggested enrichment of the PD-1/PD-L1 signaling pathway in the lnc-GLYATL2-2 high-expression group, and GO and KEGG analyses revealed that lnc-GLYATL2-2 was associated with cellular immune signaling regulation. Lnc-GLYATL2-2 has not been reported in other

tumors, and our study indicated that high expression of lnc-GLYATL2-2 can upregulate PD-L1 expression in chordoma cells, which in turn induces a suppressive immune microenvironment in chordoma and mediates immune escape and malignant progression of the tumor.

Based on earlier studies of malignant melanoma, distinct patterns of PD-L1 expression and TILs were described, and the tumor immune microenvironment (TIME) was classified into four different types to better define the immune status and predict tumor response and nonresponse or resistance to anti-PD therapy [49-51]. According to this classification, tumors can be classified into four types according to the presence of PDL1 expression and TILs (mainly composed of $CD8^+$ T cells): $PDL1^-/TIL^-$ (type I), $PDL1^+/TIL^+$ (type II), $PDL1^-/TIL^+$ (type III), and $PDL1^+/TIL^-$ (type IV) [52-54]. The above four types of TIMEs were present in our cohort of IC patients, implying noticeable heterogeneity in the chordoma immune microenvironment. In this work, we discovered a significant positive correlation between the degree of PD-L1 expression and the total number of infiltrating lymphocytes in the TIME. This finding suggested that the type II immune microenvironment may dominate chordoma. This subtype of the TIME is recognized as a paradigm of tumor immune escape and adaptive resistance mediated by the PDL1-PD1 pathway, suggesting that anti-PD therapy may have promising clinical applications in the treatment of chordoma. In support of these findings, a higher TIDE score was also observed in the lnc-GLYATL2-2 high expression subgroup, demonstrating that patients with ICs are unable to benefit from immunotherapy.

ELAVL1 is an established post-transcriptional regulator known for its role in promoting cancer progression and is frequently overexpressed in various malignancies. Previous studies have shown that circPABPN1 binds to ELAVL1, inhibiting its binding to PABPN1 mRNA and thereby suppressing the translation of this protein [55]. Additionally, another investigation revealed that circAGO2 physically interacts with ELAVL1, enhancing its activation and facilitating its enrichment in the 3'-UTR of target genes. This process reduces AGO2 binding and represses AGO2/miRNA-mediated gene silencing [56]. In our study, we present compelling evidence that lnc-GLYATL2-2 acts as an RNA-binding protein sponge, leading to the redistribution of ELAVL1 in the nuclear-cytoplasmic compartment. Notably, the 3'-UTR of PD-L1 mRNA contains multiple binding sites for ELAVL1, which renders ELAVL1 capable of stabilizing PD-L1 mRNA transcription.

Inherent mechanisms of resistance to immunotherapy involve various factors, such as decreased expression of tumor antigens, impaired antigen presentation, constitutive expression of PD-L1, and dysfunction of T cells [57]. In our study, we illustrated that high lnc-GLYATL2-2 expression triggers the upregulation of PD-L1 in chordoma cells. This upregulation, in turn, leads to constitutive enhancement of the immune checkpoint marker lnc-GLYATL2-2/PD-L1, contributing to the inactivation of antitumor T cells and ultimately resulting in a diminished response to anti-PD therapy. These findings uncover the involvement of lncRNA-mediated tumor immunosuppression and resistance to immunotherapy and provide valuable insights for enhancing the efficacy of immunotherapy in patients with ICs.

As shown in many oncomolecular biology studies, chordoma genesis and progression are associated with numerous oncogenic signaling pathways, encompassing a range of critical molecules, such as Brachyury, SMARCB1, survivin, and DEPDC1B [58-61]. Pharmaceutical products targeting these molecular candidates are also being continuously developed. However, no recognized agents have shown outstanding efficacy in the treatment of chordoma. Our research reveals the heterogeneity of the tumor microenvironment in chordoma patients, which may also be challenging for the development of anticancer medications. In addition, our study relied only on bulk RNA-seq and histopathological staining and lacked a more comprehensive analysis and discussion of the intra- and intertumor heterogeneity of chordomas. Moreover, subsequent studies are anticipated to reveal more detailed molecular mechanisms of the lnc-GLYATL2-2/PD-L1 axis in modulating the immune microenvironment of chordoma. Simultaneously, a deeper theoretical basis for immunotherapy involving ICs will be established.

## Conclusion

Lnc-GLYATL2-2 is a novel long noncoding RNA overexpressed in intracranial chordomas and is associated with poor patient prognosis. Our study suggested that lnc-GLYATL2-2 can act as a regulator to manipulate PD-L1 expression in chordomas. The expression of the lnc-GLYATL2-2/PD-L1 axis correlates with infiltrating lymphocyte subsets in the tumor microenvironment. At the molecular level, the upregulation of lnc-GLYATL2-2 can lead to changes in the nuclear-cytoplasmic distribution of the RBP ELAVL1. An increase in the cytoplasmic level of ELAVL1 allows increased binding to the PD-L1 mRNA 3'UTR, thereby maintaining its stability. Additionally, lnc-GLYATL2-2 can directly bind to the PD-L1 protein, resulting in the maintenance of high PD-L1 expression in chordoma cells (**Figure 6B**). In addition, high expression of lnc-GLYATL2-2 predicts increased sensitivity to immunotherapy in ICs patients. Thus, our study reveals the function and clinical significance of lnc-GLYATL2-2 in ICs, providing a solid foundation for IC immunotherapy.

## Acknowledgements

We would like to acknowledge our lab colleagues for their support in the development of this article. This work was supported by the National Science Foundation of China (Nos. 82101439, 82203855) and the Shanghai Sailing Program (No. 21YF1449900).

Written informed consent was obtained from all enrolled patients.

## Disclosure of conflict of interest

None.

## Abbreviations

ICs, Intracranial chordomas; LncRNAs, Long non-coding RNAs; qRT-PCR, real-time quantitative reverse transcription PCR; IHC, Immunohistochemistry; PD-L1, programmed death ligand 1; PD-1, programmed death receptor-1; TILs, tumor-infiltrating lymphocytes; GSEA, Gene Set Enrichment Analysis; TIDE, Tumor Immune Dysfunction and Exclusion; LRFS, local recurrence-free survival; OS, overall survival.

**Address correspondence to:** Yang Jiang, Department of Neurosurgery, Shanghai Tenth People's Hospital, Tongji University School of Medicine, Shanghai 200072, China. E-mail: windjy0523@qq.com; Li Li, Hospital for Chronic Neurological Diseases, Xi'an International Meidical Center Hospital Affiliated to Northwest University, Xi'an 710000, Shaanxi, China. E-mail: lilee@263.net

## References

[1] Whelan JS and Davis LE. Osteosarcoma, chondrosarcoma, and chordoma. J Clin Oncol 2018; 36: 188-193.
[2] Walcott BP, Nahed BV, Mohyeldin A, Coumans JV, Kahle KT and Ferreira MJ. Chordoma: current concepts, management, and future directions. Lancet Oncol 2012; 13: e69-76.
[3] Levine AB, Wong D, Fatehi M and Yip S. Ependymoma and chordoma. Neurosurgery 2020; 87: 860-870.
[4] Kremenevski N, Schlaffer SM, Coras R, Kinfe TM, Graillon T and Buchfelder M. Skull base chordomas and chondrosarcomas. Neuroendocrinology 2020; 110: 836-847.
[5] Zou MX, Lv GH, Zhang QS, Wang SF, Li J and Wang XB. Prognostic factors in skull base chordoma: a systematic literature review and meta-analysis. World Neurosurg 2018; 109: 307-327.
[6] Frezza AM, Botta L, Trama A, Dei Tos AP and Stacchiotti S. Chordoma: update on disease, epidemiology, biology and medical therapies. Curr Opin Oncol 2019; 31: 114-120.
[7] Passer JZ, Alvarez-Breckenridge C, Rhines L, DeMonte F, Tatsui C and Raza SM. Surgical management of skull base and spine chordomas. Curr Treat Options Oncol 2021; 22: 40.
[8] Ulici V and Hart J. Chordoma. Arch Pathol Lab Med 2022; 146: 386-395.
[9] Kim TK, Vandsemb EN, Herbst RS and Chen L. Adaptive immune resistance at the tumour site: mechanisms and therapeutic opportunities. Nat Rev Drug Discov 2022; 21: 529-540.
[10] Rosenberg SA. Decade in review-cancer immunotherapy: entering the mainstream of cancer treatment. Nat Rev Clin Oncol 2014; 11: 630-632.
[11] Kalbasi A and Ribas A. Tumour-intrinsic resistance to immune checkpoint blockade. Nat Rev Immunol 2020; 20: 25-39.
[12] Uszczynska-Ratajczak B, Lagarde J, Frankish A, Guigó R and Johnson R. Towards a complete map of the human long non-coding RNA transcriptome. Nat Rev Genet 2018; 19: 535-548.
[13] Ransohoff JD, Wei Y and Khavari PA. The functions and unique features of long intergenic non-coding RNA. Nat Rev Mol Cell Biol 2018; 19: 143-157.
[14] Tan YT, Lin JF, Li T, Li JJ, Xu RH and Ju HQ. LncRNA-mediated posttranslational modifica-

tions and reprogramming of energy metabolism in cancer. Cancer Commun (Lond) 2021; 41: 109-120.
[15] Bhan A, Soleimani M and Mandal SS. Long noncoding RNA and cancer: a new paradigm. Cancer Res 2017; 77: 3965-3981.
[16] Bach DH and Lee SK. Long noncoding RNAs in cancer cells. Cancer Lett 2018; 419: 152-166.
[17] Lv Y, Lv Y, Wang Z, Yuan K and Zeng Y. Noncoding RNAs as sensors of tumor microenvironmental stress. J Exp Clin Cancer Res 2022; 41: 224.
[18] Park EG, Pyo SJ, Cui Y, Yoon SH and Nam JW. Tumor immune microenvironment lncRNAs. Brief Bioinform 2022; 23: bbab504.
[19] Huang D, Chen J, Yang L, Ouyang Q, Li J, Lao L, Zhao J, Liu J, Lu Y, Xing Y, Chen F, Su F, Yao H, Liu Q, Su S and Song E. NKILA lncRNA promotes tumor immune evasion by sensitizing T cells to activation-induced cell death. Nat Immunol 2018; 19: 1112-1125.
[20] Li G, Kryczek I, Nam J, Li X, Li S, Li J, Wei S, Grove S, Vatan L, Zhou J, Du W, Lin H, Wang T, Subramanian C, Moon JJ, Cieslik M, Cohen M and Zou W. LIMIT is an immunogenic lncRNA in cancer immunity and immunotherapy. Nat Cell Biol 2021; 23: 526-537.
[21] Pereira B, Billaud M and Almeida R. RNA-binding proteins in cancer: old players and new actors. Trends Cancer 2017; 3: 506-528.
[22] Wu X and Xu L. The RNA-binding protein HuR in human cancer: a friend or foe? Adv Drug Deliv Rev 2022; 184: 114179.
[23] Chen H, Zhang K, Wu G, Song D, Chen K and Yang H. Low expression of PHLPP1 in sacral chordoma and its association with poor prognosis. Int J Clin Exp Pathol 2015; 8: 14741-14748.
[24] Fernandez-Miranda JC, Gardner PA, Snyderman CH, Devaney KO, Mendenhall WM, Suárez C, Rinaldo A and Ferlito A. Clival chordomas: a pathological, surgical, and radiotherapeutic review. Head Neck 2014; 36: 892-906.
[25] Luo P, Wang X, Zhou J, Li L and Jing Z. C-Cbl and Cbl-b expression in skull base chordomas is associated with tumor progression and poor prognosis. Hum Pathol 2018; 74: 129-134.
[26] Wang L, Wu Z, Tian K, Wang K, Li D, Ma J, Jia G, Zhang L and Zhang J. Clinical features and surgical outcomes of patients with skull base chordoma: a retrospective analysis of 238 patients. J Neurosurg 2017; 127: 1257-1267.
[27] Li B and Dewey CN. RSEM: accurate transcript quantification from RNA-Seq data with or without a reference genome. BMC Bioinformatics 2011; 12: 323.
[28] Jiang Y, Han S, Cheng W, Wang Z and Wu A. NFAT1-regulated IL6 signalling contributes to aggressive phenotypes of glioma. Cell Commun Signal 2017; 15: 54.
[29] Hutterer M, Knyazev P, Abate A, Reschke M, Maier H, Stefanova N, Knyazeva T, Barbieri V, Reindl M, Muigg A, Kostron H, Stockhammer G and Ullrich A. Axl and growth arrest-specific gene 6 are frequently overexpressed in human gliomas and predict poor prognosis in patients with glioblastoma multiforme. Clin Cancer Res 2008; 14: 130-138.
[30] Remmele W and Schicketanz KH. Immunohistochemical determination of estrogen and progesterone receptor content in human breast cancer. Computer-assisted image analysis (QIC score) vs. subjective grading (IRS). Pathol Res Pract 1993; 189: 862-866.
[31] Zou MX, Peng AB, Lv GH, Wang XB, Li J, She XL and Jiang Y. Expression of programmed death-1 ligand (PD-L1) in tumor-infiltrating lymphocytes is associated with favorable spinal chordoma prognosis. Am J Transl Res 2016; 8: 3274-3287.
[32] Bellmunt J, Mullane SA, Werner L, Fay AP, Callea M, Leow JJ, Taplin ME, Choueiri TK, Hodi FS, Freeman GJ and Signoretti S. Association of PD-L1 expression on tumor-infiltrating mononuclear cells and overall survival in patients with urothelial carcinoma. Ann Oncol 2015; 26: 812-817.
[33] Sato E, Olson SH, Ahn J, Bundy B, Nishikawa H, Qian F, Jungbluth AA, Frosina D, Gnjatic S, Ambrosone C, Kepner J, Odunsi T, Ritter G, Lele S, Chen YT, Ohtani H, Old LJ and Odunsi K. Intraepithelial CD8+ tumor-infiltrating lymphocytes and a high CD8+/regulatory T cell ratio are associated with favorable prognosis in ovarian cancer. Proc Natl Acad Sci U S A 2005; 102: 18538-18543.
[34] Zhang Y and Zhang Z. The history and advances in cancer immunotherapy: understanding the characteristics of tumor-infiltrating immune cells and their therapeutic implications. Cell Mol Immunol 2020; 17: 807-821.
[35] Shergold AL, Millar R and Nibbs RJB. Understanding and overcoming the resistance of cancer to PD-1/PD-L1 blockade. Pharmacol Res 2019; 145: 104258.
[36] Jiang P, Gu S, Pan D, Fu J, Sahu A, Hu X, Li Z, Traugh N, Bu X, Li B, Liu J, Freeman GJ, Brown MA, Wucherpfennig KW and Liu XS. Signatures of T cell dysfunction and exclusion predict cancer immunotherapy response. Nat Med 2018; 24: 1550-1558.
[37] Patsoukis N, Wang Q, Strauss L and Boussiotis VA. Revisiting the PD-1 pathway. Sci Adv 2020; 6: eabd2712.
[38] Yi M, Zheng X, Niu M, Zhu S, Ge H and Wu K. Combination strategies with PD-1/PD-L1

blockade: current advances and future directions. Mol Cancer 2022; 21: 28.
[39] Pauken KE, Torchia JA, Chaudhri A, Sharpe AH and Freeman GJ. Emerging concepts in PD-1 checkpoint biology. Semin Immunol 2021; 52: 101480.
[40] Riley RS, June CH, Langer R and Mitchell MJ. Delivery technologies for cancer immunotherapy. Nat Rev Drug Discov 2019; 18: 175-196.
[41] Ott PA, Hu Z, Keskin DB, Shukla SA, Sun J, Bozym DJ, Zhang W, Luoma A, Giobbie-Hurder A, Peter L, Chen C, Olive O, Carter TA, Li S, Lieb DJ, Eisenhaure T, Gjini E, Stevens J, Lane WJ, Javeri I, Nellaiappan K, Salazar AM, Daley H, Seaman M, Buchbinder EI, Yoon CH, Harden M, Lennon N, Gabriel S, Rodig SJ, Barouch DH, Aster JC, Getz G, Wucherpfennig K, Neuberg D, Ritz J, Lander ES, Fritsch EF, Hacohen N and Wu CJ. An immunogenic personal neoantigen vaccine for patients with melanoma. Nature 2017; 547: 217-221.
[42] Gettinger S, Choi J, Hastings K, Truini A, Datar I, Sowell R, Wurtz A, Dong W, Cai G, Melnick MA, Du VY, Schlessinger J, Goldberg SB, Chiang A, Sanmamed MF, Melero I, Agorreta J, Montuenga LM, Lifton R, Ferrone S, Kavathas P, Rimm DL, Kaech SM, Schalper K, Herbst RS and Politi K. Impaired HLA class I antigen processing and presentation as a mechanism of acquired resistance to immune checkpoint inhibitors in lung cancer. Cancer Discov 2017; 7: 1420-1435.
[43] Le DT, Durham JN, Smith KN, Wang H, Bartlett BR, Aulakh LK, Lu S, Kemberling H, Wilt C, Luber BS, Wong F, Azad NS, Rucki AA, Laheru D, Donehower R, Zaheer A, Fisher GA, Crocenzi TS, Lee JJ, Greten TF, Duffy AG, Ciombor KK, Eyring AD, Lam BH, Joe A, Kang SP, Holdhoff M, Danilova L, Cope L, Meyer C, Zhou S, Goldberg RM, Armstrong DK, Bever KM, Fader AN, Taube J, Housseau F, Spetzler D, Xiao N, Pardoll DM, Papadopoulos N, Kinzler KW, Eshleman JR, Vogelstein B, Anders RA and Diaz LA Jr. Mismatch repair deficiency predicts response of solid tumors to PD-1 blockade. Science 2017; 357: 409-413.
[44] Zhang L, Xu X and Su X. Noncoding RNAs in cancer immunity: functions, regulatory mechanisms, and clinical application. Mol Cancer 2020; 19: 48.
[45] Ma H, Chang H, Yang W, Lu Y, Hu J and Jin S. A novel IFNα-induced long noncoding RNA negatively regulates immunosuppression by interrupting H3K27 acetylation in head and neck squamous cell carcinoma. Mol Cancer 2020; 19: 4.
[46] Wang QM, Lian GY, Song Y, Huang YF and Gong Y. LncRNA MALAT1 promotes tumorigenesis and immune escape of diffuse large B cell lymphoma by sponging miR-195. Life Sci 2019; 231: 116335.
[47] Zhang C, Jiang F, Su C, Xie P and Xu L. Upregulation of long noncoding RNA SNHG20 promotes cell growth and metastasis in esophageal squamous cell carcinoma via modulating ATM-JAK-PD-L1 pathway. J Cell Biochem 2019; 120: 11642-11650.
[48] Sun J, Zhang Z, Bao S, Yan C, Hou P, Wu N, Su J, Xu L and Zhou M. Identification of tumor immune infiltration-associated lncRNAs for improving prognosis and immunotherapy response of patients with non-small cell lung cancer. J Immunother Cancer 2020; 8: e000110.
[49] Teng MW, Ngiow SF, Ribas A and Smyth MJ. Classifying cancers based on T-cell infiltration and PD-L1. Cancer Res 2015; 75: 2139-2145.
[50] Zhang Y and Chen L. Classification of advanced human cancers based on tumor immunity in the MicroEnvironment (TIME) for cancer immunotherapy. JAMA Oncol 2016; 2: 1403-1404.
[51] Sznol M and Chen L. Antagonist antibodies to PD-1 and B7-H1 (PD-L1) in the treatment of advanced human cancer--response. Clin Cancer Res 2013; 19: 5542.
[52] Taube JM, Anders RA, Young GD, Xu H, Sharma R, McMiller TL, Chen S, Klein AP, Pardoll DM, Topalian SL and Chen L. Colocalization of inflammatory response with B7-h1 expression in human melanocytic lesions supports an adaptive resistance mechanism of immune escape. Sci Transl Med 2012; 4: 127ra37.
[53] Negrao MV, Skoulidis F, Montesion M, Schulze K, Bara I, Shen V, Xu H, Hu S, Sui D, Elamin YY, Le X, Goldberg ME, Murugesan K, Wu CJ, Zhang J, Barreto DS, Robichaux JP, Reuben A, Cascone T, Gay CM, Mitchell KG, Hong L, Rinsurongkawong W, Roth JA, Swisher SG, Lee J, Tsao A, Papadimitrakopoulou V, Gibbons DL, Glisson BS, Singal G, Miller VA, Alexander B, Frampton G, Albacker LA, Shames D, Zhang J and Heymach JV. Oncogene-specific differences in tumor mutational burden, PD-L1 expression, and outcomes from immunotherapy in non-small cell lung cancer. J Immunother Cancer 2021; 9: e002891.
[54] Hamada T, Soong TR, Masugi Y, Kosumi K, Nowak JA, da Silva A, Mu XJ, Twombly TS, Koh H, Yang J, Song M, Liu L, Gu M, Shi Y, Nosho K, Morikawa T, Inamura K, Shukla SA, Wu CJ, Garraway LA, Zhang X, Wu K, Meyerhardt JA, Chan AT, Glickman JN, Rodig SJ, Freeman GJ, Fuchs CS, Nishihara R, Giannakis M and Ogino S. TIME (Tumor Immunity in the MicroEnvironment) classification based on tumor *CD274* (PD-L1) expression status and tumor-infiltrat-

ing lymphocytes in colorectal carcinomas. Oncoimmunology 2018; 7: e1442999.
[55] Abdelmohsen K, Panda AC, Munk R, Grammatikakis I, Dudekula DB, De S, Kim J, Noh JH, Kim KM, Martindale JL and Gorospe M. Identification of HuR target circular RNAs uncovers suppression of PABPN1 translation by CircPABPN1. RNA Biol 2017; 14: 361-369.
[56] Chen Y, Yang F, Fang E, Xiao W, Mei H, Li H, Li D, Song H, Wang J, Hong M, Wang X, Huang K, Zheng L and Tong Q. Circular RNA circAGO2 drives cancer progression through facilitating HuR-repressed functions of AGO2-miRNA complexes. Cell Death Differ 2019; 26: 1346-1364.
[57] Vesely MD, Zhang T and Chen L. Resistance mechanisms to anti-PD cancer immunotherapy. Annu Rev Immunol 2022; 40: 45-74.
[58] Sharifnia T, Wawer MJ, Chen T, Huang QY, Weir BA, Sizemore A, Lawlor MA, Goodale A, Cowley GS, Vazquez F, Ott CJ, Francis JM, Sassi S, Cogswell P, Sheppard HE, Zhang T, Gray NS, Clarke PA, Blagg J, Workman P, Sommer J, Hornicek F, Root DE, Hahn WC, Bradner JE, Wong KK, Clemons PA, Lin CY, Kotz JD and Schreiber SL. Small-molecule targeting of brachyury transcription factor addiction in chordoma. Nat Med 2019; 25: 292-300.
[59] Li M, Shen Y, Xiong Y, Wang S, Li C, Bai J and Zhang Y. Loss of SMARCB1 promotes autophagy and facilitates tumour progression in chordoma by transcriptionally activating ATG5. Cell Prolif 2021; 54: e13136.
[60] Wang L, Tang L, Xu R, Ma J, Tian K, Liu Y, Lu Y, Wu Z and Zhu X. DEPDC1B regulates the progression of human chordoma through UBE2T-mediated ubiquitination of BIRC5. Cell Death Dis 2021; 12: 753.
[61] Ma J, Tian K, Du J, Wu Z, Wang L and Zhang J. High expression of survivin independently correlates with tumor progression and mortality in patients with skull base chordomas. J Neurosurg 2019; 132: 140-149.

**Supplementary Table 1.** RNAi sequences applied in this study

| Gene | Target sequences |
|---|---|
| lnc-GLYATL2-2-KD1 | 5'-CAGATTCTGTCAACCACATTTCATA-3' |
| lnc-GLYATL2-2-KD2 | 5'-GAGCCACTTTGACAATCGTTATATA-3' |
| ELAVL1-KD1 | 5'-TCGGGAGAACGAATTTGATCGTCAA-3' |
| ELAVL1-KD2 | 5'-CAGCATTGGTGAAGTTGAATCTGCA-3' |
| siRNA-NC | 5'-ACGUGACACGUUCGGAGAA-3' |

**Supplementary Table 2.** The RT-qPCR primers in this research

| Gene | Primers sequences | |
|---|---|---|
| GAPDH | Forward | 5'-TGACCACAGTCCATGCCATCAC-3' |
| | Reverse | 5'-CGCCTGCTTCACCACCTTCTTG-3' |
| Lnc-GLYATL2-2 | Forward | 5'-TCGCTGAAGATACAACTGTTAGTCCAA-3' |
| | Reverse | 5'-CTGCTGTGAGTTCTGCCTACTTGAT-3' |
| PD-L1 | Forward | 5'-GCTATGGTGGTGCCGACTACAAG-3' |
| | Reverse | 5'-AACGGAAGATGAATGTCAGTGCTACA-3' |
| PD-L1-3'UTR | Forward | 5'-CTGAGCGTGACAAGAGGAAGGAATG-3' |
| | Reverse | 5'-CACAACCACACTCACATGACAAGAAGA-3' |

**Supplementary Table 3.** Thevantibody information used in this research

| | Antibodies | Sourse |
|---|---|---|
| Western blot | PD-L1 | Abcam |
| | ELAVL1 | Abcam |
| | β-actin | Cell signaling techology |
| | Lamin B1 | Cell signaling techology |
| RIP | PD-L1 | Abcam |
| | ELAVL1 | Abcam |
| IHC | CD4 | Abcam |
| | CD8 | Abcam |
| | Foxp3 | Abcam |
| | PD-1 | Abcam |
| | PD-L1 | Abcam |
| IF | PD-L1 | Abcam |
| | ELAVL1 | Abcam |

A

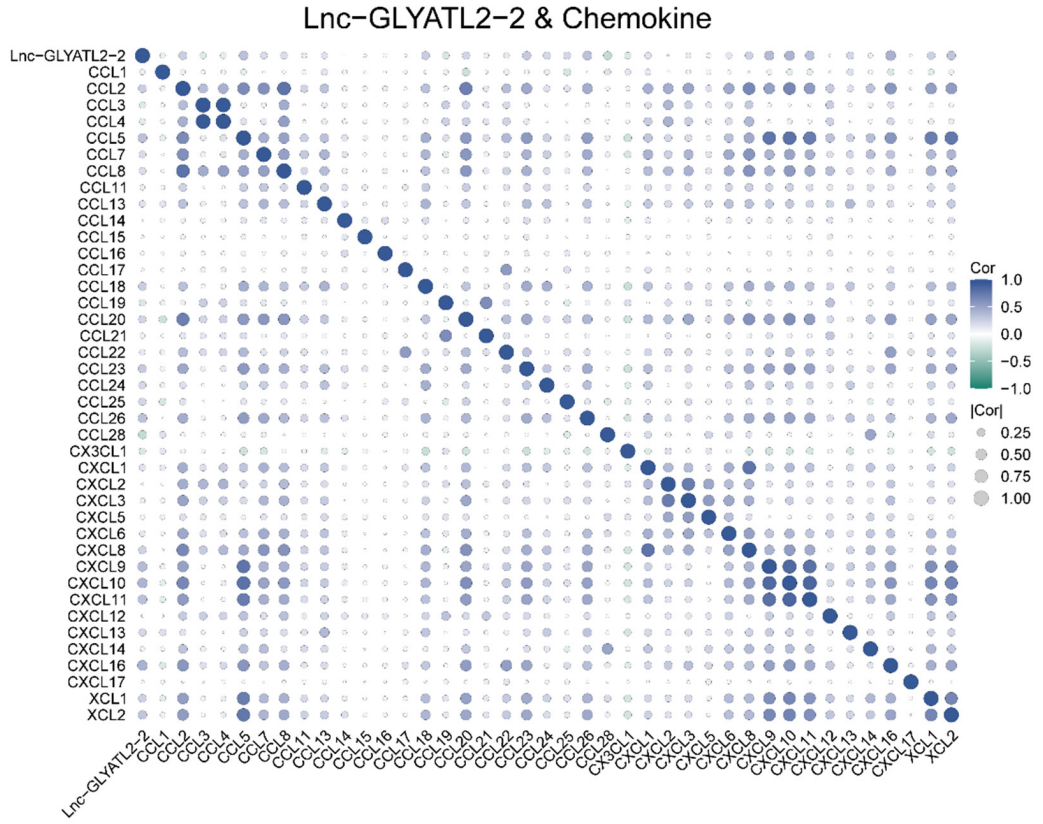
Lnc−GLYATL2−2 & Chemokine
Lnc−GLYATL2−2
CCL1
CCL2
CCL3
CCL4
CCL5
CCL7
CCL8
CCL11
CCL13
CCL14
CCL15
CCL16
CCL17
CCL18
CCL19
CCL20
CCL21
CCL22
CCL23
CCL24
CCL25
CCL26
CCL28
CX3CL1
CXCL1
CXCL2
CXCL3
CXCL5
CXCL6
CXCL8
CXCL9
CXCL10
CXCL11
CXCL12
CXCL13
CXCL14
CXCL16
CXCL17
XCL1
XCL2
Cor
1.0
0.5
0.0
−0.5
−1.0
|Cor|
0.25
0.50
0.75
1.00

B

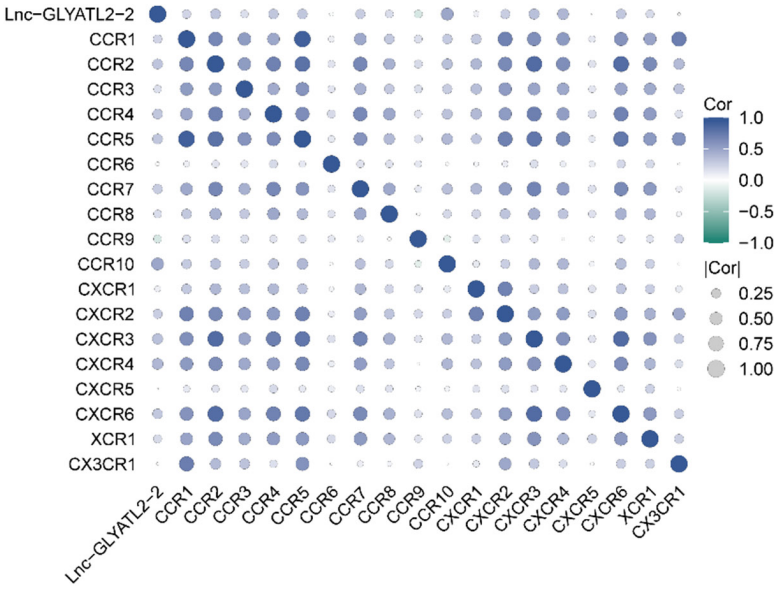
Lnc−GLYATL2−2 & Chemokine receptor
Lnc−GLYATL2−2
CCR1
CCR2
CCR3
CCR4
CCR5
CCR6
CCR7
CCR8
CCR9
CCR10
CXCR1
CXCR2
CXCR3
CXCR4
CXCR5
CXCR6
XCR1
CX3CR1
Cor
1.0
0.5
0.0
−0.5
−1.0
|Cor|
0.25
0.50
0.75
1.00

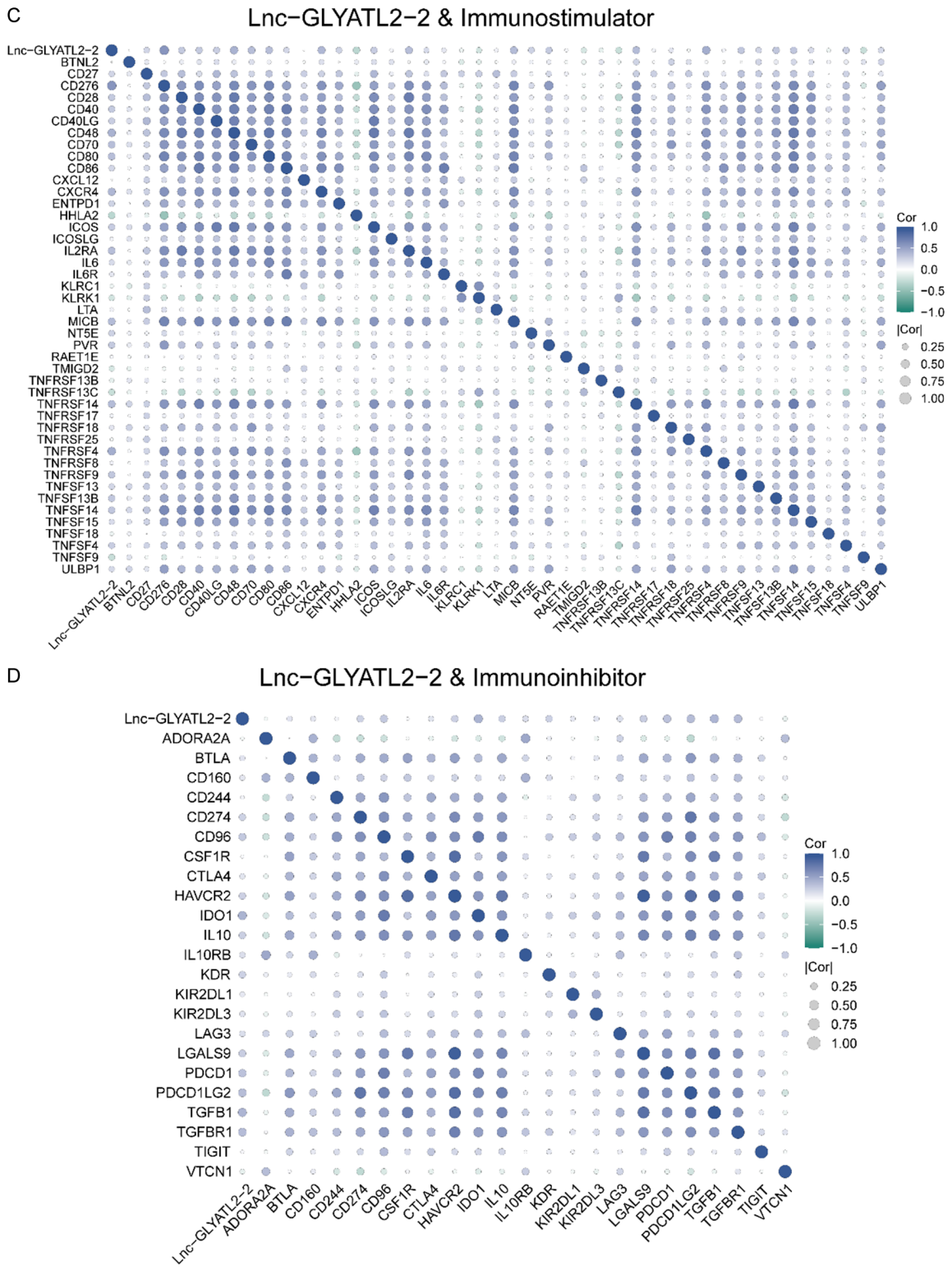


**Supplementary Figure 1.** The correlation between the lnc-GLYATL2-2 and immunomodulators in ICs. Correlation between lnc-GLYATL2-2 and immunomodulator subsets: chemokines (A), chemokine receptors (B), immunostimulators (C), and immunoinhibitors (D). *P < 0.05; **P < 0.01; ***P < 0.001; ns, no significance.

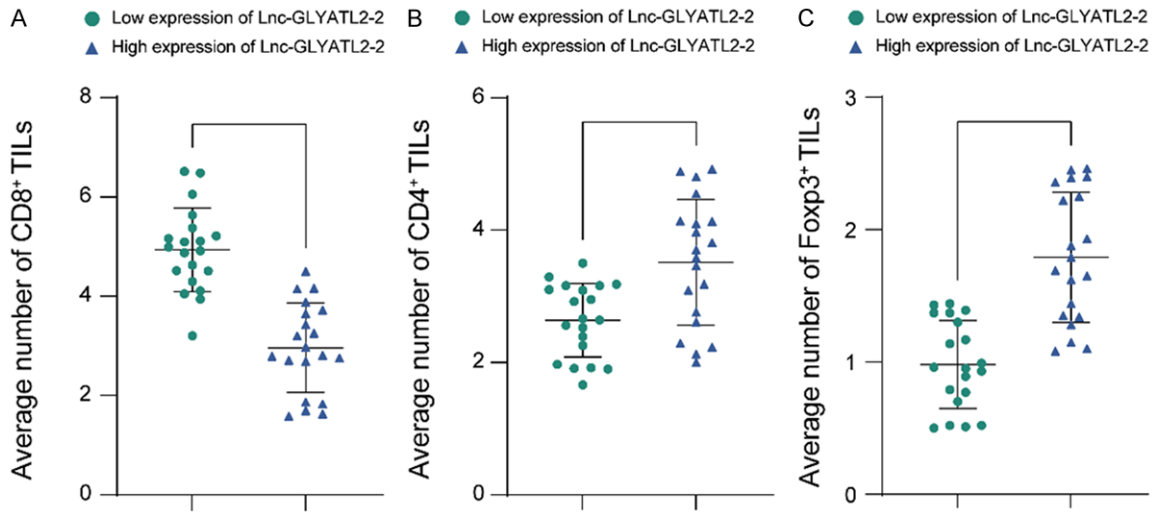


**Supplementary Figure 2.** The statistics analysis the extent of infiltration of CD8, CD4, and Foxp3 TILs in different lnc-GLYATL2-2 expression patterns of ICs. (A-C) The number of $CD8^+$ TILs (A), $CD4^+$ TILs (B), and $Foxp3^+$ TILs (C) in ICs with different lnc-GLYATL2-2 high and low groups. All data are presented as the mean ± SD (three independent experiments). *P < 0.05; **P < 0.01; ***P < 0.001; ns, no significance.

**Supplementary Table 4.** The score of ELAVL1 binding site in PD-L1 mRNA 3'UTR

| Sequence name | Sequence | Score |
|---|---|---|
| ENST00000381577.4 | AGCACGUAUUUUUAAAAUUUUUUUCCUAAAUAGUAACACAUUGUAUGUCUGCUGUGUACUUUGCUAUUUUUAUUUAUUUUAGUGUUUCUUAUAUAGCAGAU | 0.999977 |
| ENST00000381577.4 | CGUAAAUGGCAUAGGCAGAGAUGAUACCUAAUUCUGCAUUUGAUUGUCACUUUUUGUACCUGCAUUAAUUUAAUAAAAUAUUCUUAUUUAUUUUGUUACUU | 0.9920697 |
| ENST00000381577.4 | UCCAGCAUUGGAACUUCUGAUCUUCAAGCAGGGAUUCUCAACCUGUGGUUUAGGGGUUCAUCGGGGCUGAGCGUGACAAGAGGAAGGAAUGGGCCCGUGGG | 0.6723153 |
| ENST00000381577.4 | CAUAAUCUCAUUUCAUCGCUGUAACCACCCUGUUGUGAUAACCACUAUUAUUUUACCCAUCGUACAGCUGAGGAAGCAAACAGAUUAAGUAACUUGCCCAA | 0.5500254 |
| ENST00000381577.4 | ACCAGUAAAUAGCAGACCUCAGACUGCCACCCACUGUCCUUUUAUAAUACAAUUUACAGCUAUAUUUUACUUUAAGCAAUUCUUUUAUUCAAAAACCAUUU | 0.51995325 |
| ENST00000381577.4 | GGAAUGAAUUUGAAGUUCCCAGGGCUGAGGAUCCAUGCCUUCUUUGUUUCUAAGUUAUCUUUCCCAUAGCUUUUCAUUAUCUUUCAUAUGAUCCAGUAUAU | 0.46425372 |
| ENST00000381577.4 | GGUACACCAGCAUGUCCAUUUUCUUGUUUAUUUUGUGUUUAAUAAAAUGUUCAGUUUAACAUCCC | 0.4484867 |
| ENST00000381577.4 | GCCAAUGUGGUCUGGGACGGUUGGAUAUACUUAAACAUCUUAAUAAUCAGAGUAAUUUUCAUUUACAAAGAGAGGUCGGUACUUAAAAUAACCCUGAAAAA | 0.4128065 |
| ENST00000381577.4 | AUGGGCUCUCCAGGGUGCACUGAGUCAAUCUAGUCCUAAAAAGCAAUCUUAUUAUUAACUCUGUAUGACAGAAUCAUGUCUGGAACUUUUGUUUUCUGCUU | 0.41141677 |
| ENST00000381577.4 | GUUAAAUAUGUCCUACAUAUACAUUUAGACAACCACCAUUUGUUAAGUAUUUGCUCUAGGACAGAGUUUGGAUUUGUUUAUGUUUGCUCAAAAGGAGACCC | 0.40384388 |
| ENST00000381577.4 | UGACUGAGAGUCUCAGUGUUGGAACGGGACAGUAUUUAUGUAUGAGUUUUUCCUAUUUAUUUUGAGUCUGUGAGGUCUUCUUGUCAUGUGAGUGUGGUUGU | 0.39318228 |
| ENST00000381577.4 | CUGUCUUUUCUAUUUAAAUGCCACUAAAUUUUAAAUUCAUACCUUUCCAUGAUUCAAAAUUCAAAAGAUCCCAUGGGAGAUGGUUGGAAAAUCUCCACUUC | 0.38921195 |
| ENST00000381577.4 | UAACACUGGAAUUCCUUUUCUAGCAUUAUAUUUAUUCCUGAUUUGCCUUUGCCAUAUAAUCUAAUGCUUGUUUAUAUAGUGUCUGGUAUUGUUUAACAGUU | 0.35475737 |
| ENST00000381577.4 | UAAUACUCUGGUUGACCUAAUCUUAUUCUCAGACCUCAAGUGUCUGUGCAGUAUCUGUUCCAUUUAAAUAUCAGCUUUACAAUUAUGUGGUAGCCUACACA | 0.34180683 |
| ENST00000381577.4 | UGAGCAAGGCACAUAGUCUACUCAGUCUAUUCCUAAGUCCUAACUCCUCCUUGUGGUGUUGGAUUUGUAAGGCACUUUAUCCCUUUUGUCUCAUGUUUCAU | 0.33427557 |
| ENST00000381577.4 | UAUUUGUAAGGUGCUUGGUCUCCUCUAUAACUACAAGUAUACAUUGGAAGCAUAAAGAUCAAACCGUUGGUUGCAUAGGAUGUCACCUUUAUUUAACCCAU | 0.33425736 |
| ENST00000381577.4 | AUGCAGGCAAUGUGGGACUUAAAAGGCCCAAGCACUGAAAAUGGAACCUGGCGAAAGCAGAGGAGGAGAAUGAAGAAAGAUGGAGUCAAACAGGGAGCCUG | 0.32872617 |
| ENST00000381577.4 | GAGGGAGACCUUGAUACUUUCAAAUGCCUGAGGGGCUCAUCGACGCCUGUGACAGGGAGAAAGGAUACUUCUGAACAAGGAGCCUCCAAGCAAAUCAUCCA | 0.32445472 |
| ENST00000381577.4 | UUGCUCAUCCUAGGAAGACGGGUUGAGAAUCCCUAAUUUGAGGGUCAGUUCCUGCAGAAGUGCCCUUUGCCUCCACUCAAUGCCUCAAUUUGUUUUCUGCA | 0.32399124 |
| ENST00000381577.4 | AGAUUAACAAGAAAAUGUAUUAUUACAAUUUAGUCCAGUGUCAUAGCAUAAGGAUGAUGCGAGGGGAAAACCCGAGCAGUGUUGCCAAGAGGAGGAAAUAG | 0.32140857 |
| ENST00000381577.4 | CCUGGGAGAUCCCAGAGUUUCCUUUCCCUCUUGGCCAUAUUCUGGUGUCAAUGACAAGGAGUACCUUGGCUUUGCCACAUGUCAAGGCUGAAGAAACAGUG | 0.3152861 |
| ENST00000381577.4 | AUCCUCCAAGCCAUUCAAGUUUCCUUUCCAGAAGCAACUGCUACUGCCUUUCAUUCAUAUGUUCUUCUAAAGAUAGUCUACAUUUGGAAAUGUAUGUUAAA | 0.3115083 |
| ENST00000381577.4 | UCUGUCAAGUAUAAACUUCACUUUGAUGCUGUACUUGCAAAAUCACAUUUUCUUUCUGGAAAUUCCGGCAGUGUACCUUGACUGCUAGCUACCCUGUGCCA | 0.29765502 |
| ENST00000381577.4 | GAAUGAUUUCUUUUGAAGAUAUAUUGUAGUAGAUGUUACAAUUUUGUCGCCAAACUAAACUUGCUGCUUAAUGAUUUGCUCACAUCUAGUAAAACAUGGAG | 0.2936331 |
| ENST00000381577.4 | UCUCCAACAGAGCUCCUUGUGUUAUCUGUUUGUACAUGUGCAUUUGUACAGUAAUUGGUGUGACAGUGUUCUUUGUGUGAAUUACAGGCAAGAAUUGUGGC | 0.29009 |
| ENST00000381577.4 | GAAAAGCCUCAUUCGUUGUGCUUGAACCCUUGAAUGCCACCAGCUGUCAUCACUACACAGCCCUCCUAAGAGGCUUCCUGGAGGUUUCGAGAUUCAGAUGC | 0.2850334 |
| ENST00000381577.4 | AUUAAGUGCCCUUGCAAUAUCAAUCGCUGUGCCAGGCAUUGAAUCUACAGAUGUGAGCAAGACAAAGUACCUGUCCUCAAGGAGCUCAUAGUAUAAUGAGG | 0.2744671 |

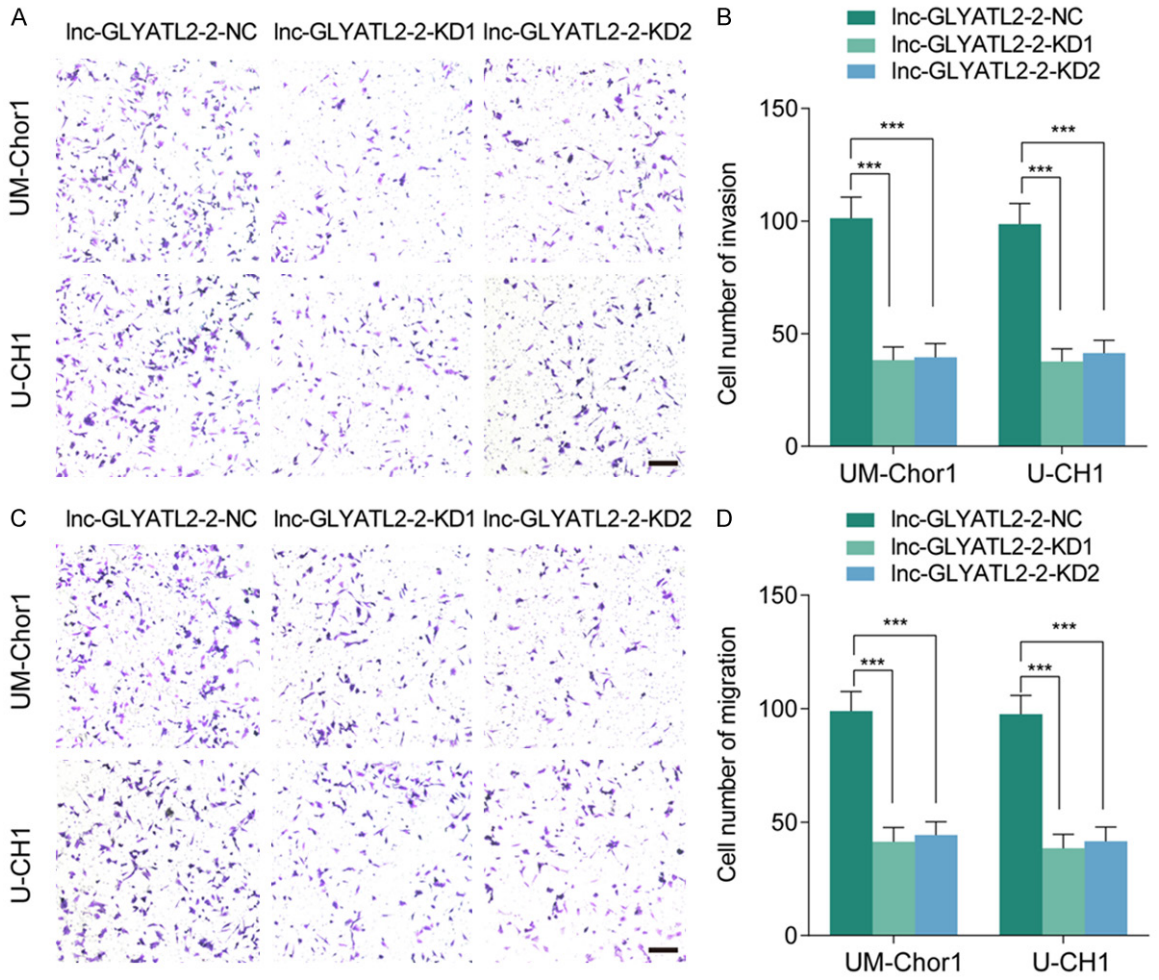


**Supplementary Figure 3.** The varied expression of lnc-GLYATL2-2 can affect the invasive and migratory abilities of chordoma cells in vitro. (A-D) Invasion (A, B) and migration (C, D) assay showed the invasive and migratory abilities of chordoma cells were weakened after lnc-GLYATL2-2 knockdown in UM-Chor1 and U-CH1. Scale bar =100 μm. All data are presented as the mean ± SD (three independent experiments). *P < 0.05; **P < 0.01; ***P < 0.001; ns, no significance.